



Crosstalk between glucocorticoid and mineralocorticoid receptors boosts glucocorticoid-induced killing of multiple myeloma cells

Dorien Clarisse^{1,2,3} · Stefan Prekovic⁴ · Philip Vlummens⁵ · Eleni Staessens^{1,2,3} · Karlien Van Wesemael^{1,5} · Jonathan Thommis^{1,2} · Daria Fijalkowska¹ · Guillaume Acke⁶ · Wilbert Zwart⁷ · Ilse M. Beck⁸ · Fritz Offner^{3,5} · Karolien De Bosscher^{1,2,3}

Received: 22 May 2023 / Revised: 11 July 2023 / Accepted: 27 July 2023 / Published online: 14 August 2023
© The Author(s) 2023

Abstract

The glucocorticoid receptor (GR) is a crucial drug target in multiple myeloma as its activation with glucocorticoids effectively triggers myeloma cell death. However, as high-dose glucocorticoids are also associated with deleterious side effects, novel approaches are urgently needed to improve GR action in myeloma. Here, we reveal a functional crosstalk between GR and the mineralocorticoid receptor (MR) that plays a role in improved myeloma cell killing. We show that the GR agonist dexamethasone (Dex) downregulates MR levels in a GR-dependent way in myeloma cells. Co-treatment of Dex with the MR antagonist spironolactone (Spi) enhances Dex-induced cell killing in primary, newly diagnosed GC-sensitive myeloma cells. In a relapsed GC-resistant setting, Spi alone induces distinct myeloma cell killing. On a mechanistic level, we find that a GR–MR crosstalk likely arises from an endogenous interaction between GR and MR in myeloma cells. Quantitative dimerization assays show that Spi reduces Dex-induced GR–MR heterodimerization and completely abolishes Dex-induced MR–MR homodimerization, while leaving GR–GR homodimerization intact. Unbiased transcriptomics analyses reveal that *c-myc* and many of its target genes are downregulated most by combined Dex-Spi treatment. Proteomics analyses further identify that several metabolic hallmarks are modulated most by this combination treatment. Finally, we identified a subset of Dex-Spi downregulated genes and proteins that may predict prognosis in the CoMMpass myeloma patient cohort. Our study demonstrates that GR–MR crosstalk is therapeutically relevant in myeloma as it provides novel strategies for glucocorticoid-based dose-reduction.

Keywords Glucocorticoids · Glucocorticoid receptor · Mineralocorticoid receptor · Nuclear receptor crosstalk · Multiple myeloma

Introduction

More than 10% of all patients with hematological malignancies are diagnosed with multiple myeloma, which is a plasma cell cancer that is localized in the bone marrow

Ilse M. Beck and Fritz Offner contributed equally to this work.

✉ Karolien De Bosscher
karolien.debosscher@vib-ugent.be

¹ VIB Center for Medical Biotechnology,
Technologiepark-Zwijnaarde 75, 9052 Ghent, Belgium

² Department of Biomolecular Medicine, Ghent University,
Ghent, Belgium

³ Cancer Research Institute Ghent (CRIG), Ghent, Belgium

⁴ Center for Molecular Medicine, University Medical Center
Utrecht, Utrecht, The Netherlands

⁵ Department of Internal Medicine and Pediatrics, Ghent
University Hospital, Ghent, Belgium

⁶ Department of Chemistry, Ghent University, Ghent, Belgium

⁷ Division of Oncogenomics, Oncode Institute, The
Netherlands Cancer Institute, Amsterdam, The Netherlands

⁸ Department of Health Sciences, Odisee University
of Applied Sciences, Ghent, Belgium

[1]. Despite significant advances in myeloma treatment, synthetic glucocorticoids (GCs) such as dexamethasone (Dex) remain an important pillar of the myeloma treatment protocol because of their strong anti-myeloma activities, justifying their continued use in all treatment stages [1, 2]. However, long-term use of high-dose GCs is hampered by the emergence of GC resistance and side effects including osteoporosis, hyperglycemia, muscle wasting and severe mood swings, which negatively impact patient quality-of-life and treatment adherence [3].

Both the therapeutic and unwanted effects of GCs are exerted through ligand-mediated activation of the glucocorticoid receptor (GR); a transcription factor belonging to the superfamily of ligand-activated nuclear receptors [4]. Once GCs bind to GR, the receptor undergoes a conformational change that results in a rearrangement of the Hsp90-Hsp70/40-containing multi-protein complex that aids in nuclear translocation of GR [5]. In the nucleus, ligand-activated GR can promote gene activation, which can be accomplished by GR homodimers binding to glucocorticoid response elements (GREs) of target gene promoters or enhancers [6, 7]. In contrast, GR monomers can trigger gene repression by interfering with gene expression programs of other DNA-bound transcription factors such as NF- κ B and AP-1 via, for instance, a tethering mechanism [8]. However, the dominant interaction mode between GR oligomers and other transcription factors on DNA remains a topic of debate [9–12].

The intricate interplay of GR oligomers with other nuclear receptor oligomers, also called nuclear receptor crosstalk, results in a unique gene expression profile that allows for a strengthening or weakening of each receptor's activity [13]. This crosstalk was already established for GR and estrogen receptor α (ER α) in breast cancer and for GR and androgen receptor (AR) in prostate cancer and influences therapy responsiveness [14, 15]. We serendipitously found that besides GR, the structurally closely related mineralocorticoid receptor (MR) was differentially expressed between myeloma cell lines. The impact of a possible interplay between GR and MR on GC therapy responsiveness has, however, not been studied in myeloma.

MR responds to two physiological ligands, aldosterone and cortisol, in a cell-type-dependent manner and is ubiquitously expressed [16]. This receptor regulates electrolyte balance and water homeostasis in epithelial cells, while in non-epithelial cells inappropriate MR activation triggers pro-inflammatory and profibrotic effects [17]. MR-mediated effects are counteracted by MR antagonists, such as spironolactone (Spi), which are used in the clinic for their cardiovascular and renal protective functions and to lower blood pressure [18]. Crosstalk mechanisms between GR and MR were shown in several tissues and result in the formation of GR–MR heterodimers [19–23] or even higher-order

oligomers [24, 25], thereby modulating the transcriptional activity of each receptor. Indeed, MR can inhibit or promote Dex-induced GR-mediated transcriptional activity, or vice versa, with the outcome depending on the target tissue. The Pérez team reported in 2023 that GR binding to chromatin in keratinocytes was strongly reduced in the absence of MR, which especially impacted the kinetics and magnitude of GR-mediated transcriptional activity in a gene-dependent way [23]. A study in neuroblastoma cells also supported cooperation between GR and MR, where MR augmented the magnitude of GR-mediated transcription, at least for a subset of genes, by a tethering of MR to DNA-bound GR [26]. Other studies report the opposite, with MR inhibiting GR-mediated gene transcription following GR–MR heterodimerization [27–29]. How the GC response in myeloma may be influenced by the interplay between GR and MR is still elusive.

In this study, we present a novel crosstalk mechanism between GR and MR in multiple myeloma cells that may offer a unique therapy-supportive angle for myeloma treatment. We show that GCs downregulate MR levels in a GR-dependent fashion and that inhibiting MR with Spi culminates in an enhanced Dex-induced myeloma cell killing. We further elaborate on this GR–MR crosstalk by showing that Spi reduces Dex-induced GR–MR heterodimerization and completely abolishes Dex-induced MR–MR homodimerization. Finally, we reveal the transcriptomic and proteomic signatures of the Dex-Spi combination treatment that underpin the enhanced myeloma cell killing effects and identify a subset of Dex-Spi-regulated targets that predict survival in the CoMMpass patient cohort.

Materials and methods

Cell lines and reagents

MM1.S, OPM-2, L-363, U-266 and MM1.R cells were cultured in RPMI1640 GlutaMAX and HEK293T and EA.hy926 cells in DMEM, both supplemented with 10% fetal bovine serum (FBS), 100U/mL penicillin and 0.1 mg/mL streptomycin and grown at 5% CO₂ and 37 °C. MM1.S, MM1.R and EA.hy926 were purchased from ATCC. OPM-2 was kindly provided by Prof. B. Thompson (University of Texas Medical Branch) and L-363 and U-266 cells by Prof. M. Engelhardt (Uniklinik Freiburg, Germany). HEK293T was obtained from the cytokine receptor laboratory (Ghent University). All cell lines were mycoplasma-negative (MycoAlert kit, Lonza). Experiments were performed using charcoal-stripped serum (CTS), unless otherwise specified.

Total solvent concentrations were equal in all conditions. Dex, hydrocortisone (Hcort), prednisolone (Pred), flucinolone acetonide (FA), aldosterone (Ald), RU486 and

cycloheximide (CHX) were purchased from Sigma-Aldrich and dissolved in ethanol (EtOH), unless otherwise specified. Spi and chloroquine (CQ) were obtained from Santa Cruz Biotechnology and dissolved in, respectively, EtOH and water, unless otherwise specified. MG132 was purchased from Selleck Chemicals and dissolved in DMSO.

siRNA nucleofection

MM1.S cells were transfected with siCtrl, siGR or siMR (see Supplementary Table S1) in 24-well plates by nucleofection using cell line nucleofector kit V and the nucleofector device at program X01. 48 h post-nucleofection, cells were reseeded to 96-well plates and treated for another 24 h with compounds (details in Fig. legends).

NanoBiT-based homo- and heterodimerization assays

HEK293T cells were seeded in 96-well plates in 10%FBS DMEM and transfected 24 h later with 2.5 ng pLgBiT-MR (LgBiT at N-terminus) and 2.5 ng pGR-SmBiT (SmBiT at C-terminus) for the GR-MR heterodimerization assay; or 1.5 ng pLgBiT-GR (LgBiT at N-terminus) and 1.5 ng pGR-SmBiT (SmBiT at C-terminus) for the GR-GR homodimerization assay; or 1 ng pLgBiT-MR (LgBiT at N-terminus) and 1 ng pMR-SmBiT (SmBiT at C-terminus) for the MR-MR homodimerization assay, using calcium phosphate precipitation. 24 h later, the Nano-Glo® Live Cell reagent was reconstituted (Promega) and 25 μ L was added to the transfected cells, after which the baseline luminescence was measured for 15 min (continuous-mode, 1-min intervals) using an Envision (PerkinElmer) spectrophotometer. Subsequently, ligands were added (see Fig. legends) and the luminescence was measured in a time window of 60 min (continuous-mode, 1-min intervals). Luminescence counts were normalized to baseline and set as a fold-difference versus the solvent condition (here: DMSO). The area under the curve method was used to statistically compare Dex and Dex-Spi conditions.

RT-qPCR

Total RNA was isolated using the RNeasy mini kit (Qiagen). Reverse transcription (RT) was performed using the iScript cDNA synthesis kit (Bio-Rad). The resulting cDNA served as template for the quantitative PCR (qPCR) reaction, for which Lightcycler 480 SYBR Green I Master mix (Roche diagnostics) was used (40 amplification cycles). Primer sequences are available in Supplementary Table S2. Cq values were analyzed using qBasePlus (Biogazelle) and normalized to the reference genes SDHA, RPL13A and YWHAZ.

RNA-sequencing

Total RNA was isolated using the RNeasy mini kit (Qiagen). The RNA-seq library was prepared using the Illumina TruSeq stranded mRNA library kit, followed by single-end 100-bp sequencing on an Illumina NOVASeq 600 instrument (VIB Nucleomics core), yielding 19–27 million reads per sample. Briefly, sequencing reads were quality-controlled with FastQC (version 0.11.9) and trimmed using Trim-Galore (version 0.6.6-0) to remove low-quality ends (phred score < 30) as well as adapters, followed by another quality control of the trimmed data. Thereafter, reads were pre-mapped to PhiX genome using STAR (version 2.7.6a), and the resulting PhiX-unmapped reads were aligned to the human genome GRCh38. The position-sorted output BAM files were converted to count data using HTSeq (version 0.12.4) in the ‘union’ mode. Differential gene expression analysis was performed using DESeq2 R package (version 1.34.0), using an interaction model (design formula: $c_0x_0 + c_1x_1 + c_2x_2 + c_3x_1x_2$). As input for the analysis, only genes with counts > 1 were withheld. Normalized counts were either plotted per gene or were compared for all genes, clustered, and presented as heatmaps (pheatmap package, version 1.0.12). Pairwise comparisons between differentially treated samples (e.g. Dex-Spi vs EtOH) as well as the interaction term were retrieved at a significance level of $\alpha = 0.05$, corresponding to Wald-test adjusted p -value (FDR) cutoff (p_{adj}). Volcano plots were made depicting the p_{adj} (log10 scale) in function of the log2FC for all genes with base-Mean ≥ 50 in the interaction term and each pairwise comparison of interest. Functional annotations of differentially expressed genes were performed using ingenuity pathway analysis (IPA) or gene-set enrichment analysis (GSEA, using standard parameters) [30].

Protein lysates and western blotting (WB)

Protein lysates were prepared using Totex lysis buffer, as described before [31], loaded on an SDS-PAGE gel, and blotted onto nitrocellulose membranes (Bio-Rad). The list of primary antibodies can be found in Supplementary Table S3. Note that the primary MR antibody is of a non-commercial source, and hence, different batches were used throughout the course of this research (clone 6G1, kind gift Dr. Gomez-Sanchez). As secondary antibodies, we used species-specific HRP-conjugated antibodies (cat nr: NA931, NA934, GE-Healthcare). To visualize results, Pierce ECL (Plus) (Thermo Fisher Scientific), Westernbright Quantum or Sirius (Isogen), or ECL Prime (GE Healthcare) served as chemiluminescent substrates, and signals were developed using X-ray films or imaged on a ProXima 2850 (Isogen) or Amersham 680 (GE healthcare) imaging system. Band densitometric analyses were performed using ImageJ.

Shotgun proteomics

MM1.S were treated for 24 h with compounds (see Fig. legends), after which the cells were collected by washing with ice-cold PBS and storing the cell pellets at -80°C . Four biological replicates were performed. The mass spectrometry sample preparation and computational analysis were performed as previously described [32].

Co-immunoprecipitation

Post-treatment, MM1.S or OPM-2 cells were lysed in NP-40 lysis buffer (50 mM Tris-HCl pH 8.0, 150 mM NaCl, 1% NP-40) and subjected to immunoprecipitation using anti-GR G5 antibody, as described before [33]. Briefly, cell lysates were precleared with immobilized protein A dynabeads (50 μL bead slurry, with f.c. 2 mg/mL BSA) by 1 h rotation at 4°C . Ensuing, 100–150 μg total protein was combined with anti-GR G5 antibody (sc-393232) and rotated for 1 h at 4°C , after which immobilized dynabeads (50 μL bead slurry, with f.c. 2 mg/mL BSA) were added followed by another 2 h rotation at 4°C . Following washing steps in NP-40 lysis buffer, the bead mixtures were denatured for 5 min at 95°C using 4xLaemli buffer supplemented with DTT (f.c. 200 mM). Samples were subjected to WB analyses, and anti-MR 6G1 antibody (kind gift Dr. Gomez-Sanchez) was used to assay the interaction between immunoprecipitated GR and MR.

Flow cytometry

MM1.S cells were resuspended in Annexin-binding buffer and between 10^5 and 5×10^5 cells were stained with Alexa Fluor 488 Annexin V and propidium iodide (Molecular Probes by Invitrogen). Unstained and single stained cells served as controls. Samples were measured on an Attune Nxt flow cytometer (Thermo Fisher Scientific). Data analysis was performed using FlowJo; the gating strategy is depicted in Supplementary Fig. S3b.

Cell viability assays

MM cells were seeded and treated immediately with compounds for 24 h or 72 h (see Fig. legends). Thereafter, cells were subjected to a CellTiterGlo cell viability assay (Promega), as described before [31]. Briefly, the reconstituted CellTiterGlo reagent (Promega) was added in a 1:1 ratio to the cells, and contents were mixed for 2 min on an orbital shaker. Following signal stabilization (10 min), luminescence was recorded using a Spectramax Paradigm

(Beckman Coulter), Envision or Ensign (Perkin Elmer) spectrophotometer.

Patient-derived MM cells

Sample acquisition was approved by the ethical commission of the Ghent University Hospital (EC UZG 2018/0906), and informed consent was obtained from all patients. Bone marrow aspirates were filtered through a cell strainer and mixed with a RosetteSep human MM cell enrichment cocktail (negative selection, STEMCELL Technologies). Afterward, bone marrow aspirates were diluted 1:1 with PBS (+2% FBS) and layered on a Lymphoprep gradient using SepMate tubes (STEMCELL Technologies). After centrifugation, the cells were washed twice with PBS (+2%FBS) and with a red blood cell lysis buffer (0.8% NH_4Cl , 0.1 mM EDTA, STEMCELL technologies). Thereafter, the enriched MM cells were resuspended in RPMI1640 GlutaMAX (+10%CTS) and subjected to a cell viability assay and/or RNA isolation.

Survival analysis

A publicly available dataset was used to evaluate the prognostic significance of set of genes/proteins identified via RNA-sequencing or shotgun proteomics. Specifically, the Relating Clinical Outcomes in MM to Personal Assessment of Genetic Profile (CoMMpass) trial release IA14 was used, launched by the MM research foundation (MMRF). Normalized TPM gene expression values, generated using RNA-sequencing, were downloaded alongside clinical data through the MMRF research portal (<https://research.themmr.org>). Overall survival (OS) was defined as the time from diagnosis until death from any cause or until the time point the patient was last known to be alive. In the latter case, patients were censored. Progression-free survival (PFS) delineates the time from treatment initiation until relapse or death from any cause. Patients were divided into 2 or 3 groups based on the average of their z-score normalized expression data, ranked from low to high (2 groups) or from low to medium to high (3 groups). Survival analysis of the CoMMpass cohort was performed using R (package survival, V3.5-3); statistical significance was calculated using the log-rank test. Prognostic factor analysis was done using SigCheck package (V2.28.0), running with standard parameters.

Statistical analyses

Statistical analyses were performed using GraphPad Prism 9 or R, as specified in the figure legends. Sample size calculations were not performed upfront. Experiments were performed in at least three independent repetitions, as detailed in the figure legends, except for experiments involving

patient material, which could only be performed once because of the limited culturing time and yield of the isolated primary cells. Error bars represent the standard error of the mean (SEM), except for experiments involving primary patient material, where the error bars represent the standard deviation (SD). When the means of 2 groups were compared, a two-tailed independent Student's *t*-test was used; when the means of more than 2 groups were compared, a one-way or two-way ANOVA with (Tukey's or Sidak's) multiple comparisons post-test was used, as detailed in the figure legends. Normal distribution and equality of variances were assumed. Statistical significance in survival curve estimates was calculated using the log-rank test. When $P < 0.05$, results were designated significant: * $P < 0.05$, ** $P < 0.01$, *** $P < 0.001$, **** $P < 0.0001$, ns = non-significant.

Results

Dex downregulates MR levels in a GR-dependent way

We first examined whether GCs regulate MR mRNA and protein levels (Fig. 1A, B) in five myeloma cell lines (MM1.S, OPM-2, L-363, U-266 and MM1.R) [34, 35] with different sensitivities to Dex-mediated myeloma cell killing (Fig. 1C). A 6 h Dex treatment downregulated *NR3C2* (MR) transcripts in cells showing the highest GC-inducible MM cell killing (MM1.S, OPM-2 and L-363), while in cells with virtually no GC-mediated MM cell killing (U-266 and MM1.R), *NR3C2* mRNA levels remained unchanged (Fig. 1A). MR protein levels were also downregulated in GC-sensitive MM1.S and OPM-2 cells following 24 h Dex treatment and only slightly in GC-resistant GR-negative MM1.R cells (Fig. 1B). *NR3C2* mRNA expression levels aligned in all cell lines with previously obtained RNA-sequencing data from the Keats lab (Supplementary Table S4), with OPM-2 having the highest and U-266 having the lowest *NR3C2* transcript levels. Despite that *NR3C2* mRNA is present in all myeloma cell lines (Fig. 1A, Supplementary Table S4), MR protein levels were hardly detectable via Western analyses in both U-266 and L-363 cells, indicating low MR protein expression in the latter cell lines (Fig. 1B).

Dex decreased *NR3C1* (GR) mRNA levels only in L-363 cells and thus not in the GC-inducible MM1.S and OPM-2 cells (Supplementary Fig. S1; MM1.R is *NR3C1*-negative). GR protein, however, consistently underwent homologous downregulation following 24 h Dex treatment (also known as negative feedback of GR) in all GR-containing MM cells (Fig. 1B), which agrees with several reports [31, 36–38]. Next to both receptors, we examined the Dex response of shared target genes. *TSC22D3* (GILZ) [39] and

FKBP5 mRNA levels were upregulated by Dex in all MM cells except MM1.R cells, while *SGK1* mRNA levels are decreased by Dex in MM1.S, L-363 and U-266 cells (Supplementary Fig.S1).

The dynamic behavior of this Dex-induced MR downregulation was illustrated by showing that from 3 h onwards, Dex significantly decreased *NR3C2* mRNA levels in MM1.S and OPM-2 cells; a fast regulation that was largely recapitulated at the protein level (Fig. 1D, E). In contrast to *NR3C1* mRNA levels, Dex gradually decreased GR protein levels over time (Fig. 1D, E), as shown before [31].

To confirm our observations across GCs with different potencies, we compared, ranked from high to low potency, the following ligands: Dex, fluocinolone acetonide (FA), prednisolone (Pred) and hydrocortisone (Hcort). All GCs consistently downregulated MR protein levels in MM1.S cells (Supplementary Fig.S2A). We observed a double MR band (with Dex, FA) and even multiple MR bands (with Pred, Hcort) in MM1.S, while in MM1.R only Pred and Hcort induced a clear double MR band, suggestive of post-translational modification of MR [40].

Several lines of evidence support that the Dex-induced MR protein downregulation is largely GR-dependent. First, we used the GR antagonist RU486. A Dex/RU486 combination left MR protein levels intact compared to Dex alone in MM1.S and OPM-2 cells (Fig. 1F). In addition, an siRNA-based GR knockdown in MM1.S cells showed that MR levels are at least partially protected from Dex-induced downregulation in siGR compared to siCtrl conditions (Fig. 1G), overall supporting a GR-dependent mechanism. Noteworthy, knockdown of GR was already sufficient to increase the basal MR protein levels in MM1.S cells. Thirdly, in GR-negative MM1.R cells, Dex may bind MR instead, although this was clearly not sufficient to trigger the pronounced MR downregulation that was observed in GR-positive MM1.S cells (Fig. 1B).

To investigate whether Dex lowered *NR3C2* levels post-transcriptionally, we used actinomycin D (ActD) to block de novo transcription in MM1.S cells. ActD by itself reduced *NR3C2* levels threefold compared to solvent condition, indicating that MR mRNA is unstable (Fig. 1I). Addition of Dex on top of ActD could not further reduce the residual *NR3C2* mRNA levels, suggesting that novel gene transcription is needed. Next, we evaluated whether mechanisms centered at the protein level were contributing to Dex-induced MR downregulation. The protein translation inhibitor cycloheximide (CHX), of which the activity was confirmed via β -catenin downregulation (positive control), combined with Dex did not further reduce the MR protein levels at 6 h treatment compared to Dex alone. This indicates that Dex requires novel protein synthesis to decrease MR protein levels (Fig. 1J). In addition, Dex did not lower MR protein levels via lysosomal degradation, as assessed with chloroquine

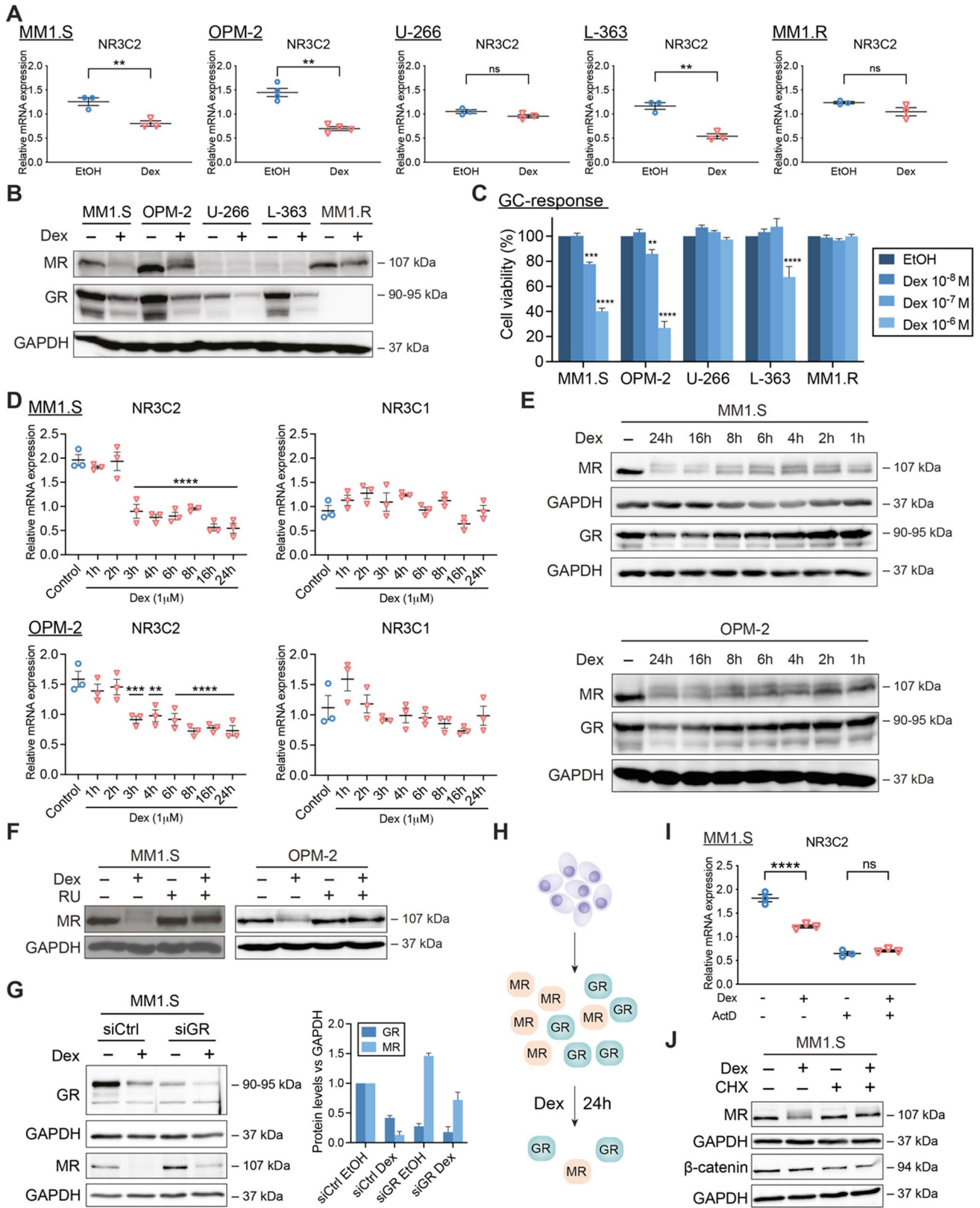


Fig. 1 GCs downregulate MR mRNA and protein levels in a GR-dependent way. **(A, B)** MM1.S, OPM-2, U-266, L-363 and MM1.R cells were treated with Dex (10^{-6} M) or solvent control (EtOH), **(A)** for 6 h, followed by RT-qPCR (all $N=3$, except OPM-2: $N=4$), assessing the mRNA levels of *NR3C2* (MR), or **(B)** for 24 h, followed by WB analysis ($N=3$). The protein levels of MR (107 kDa) and GR (90–95 kDa) were determined, with GAPDH (37 kDa) as loading control. **(C)** MM1.S, OPM-2, U-266, L-363 and MM1.R cells were treated for 72 h with a Dex concentration range (10^{-6} M– 10^{-8} M) or solvent control (EtOH, set as 100%), followed by a CelltiterGlo cell viability assay (72 h Dex range recapitulated from Figs. 2I and 3B–D). The bar plots represent the mean \pm SEM. Statistical analyses were performed using GraphPad Prism 9, using a two-way ANOVA with post hoc testing. Per cell line, 10^{-6} M Dex and 10^{-7} M Dex conditions were statistically compared to the 10^{-8} M Dex condition. **(D, E)** MM1.S or OPM-2 cells were treated for different time points with Dex (10^{-6} M) or solvent control (EtOH) followed by **(D)** RT-qPCR ($N=3$), assessing the mRNA levels of *NR3C2* (MR) and *NR3C1* (GR) and in which statistical analyses compared each time point to solvent control, or **(E)** WB analysis ($N=3$), in which the protein levels of MR (107 kDa) and GR (90–95 kDa) were determined, with GAPDH (37 kDa) as loading control. **(F)** OPM-2 and MM1.S cells were treated with Dex (10^{-6} M), RU (10^{-5} M), a combination thereof or solvent control for 24 h, followed by WB analysis ($N=3$). The protein levels of MR (107 kDa) were determined, with GAPDH (37 kDa) as loading control. **(G)** MM1.S cells were nucleofected with siCtrl (scrambled) or siGR and 48 h post-nucleofection treated for another 24 h with Dex (10^{-6} M) or solvent control, followed by WB analysis ($N=3$) and band densitometric analysis (bar plot). The latter shows the normalized GR or MR protein levels (vs. GAPDH), averaged over 3 biological replicates. **(H)** Graphical summary. In MM cells containing GR and MR protein, Dex downregulates GR protein levels and to an even higher extent MR protein levels, especially at 24 h. **(I)** MM1.S cells were treated for 3 h with Dex (10^{-6} M), ActD (1 μ g/mL), a combination thereof or solvent, followed by RT-qPCR ($N=3$), assessing the mRNA levels of *NR3C2*. **(J)** MM1.S cells were treated for 6 h with Dex (10^{-6} M), CHX (20 μ g/mL), a Dex/CHX combination or solvent control, followed by WB analysis ($N=3$) and band densitometric analysis. The protein levels of MR (107 kDa), or β -catenin (94 kDa; positive control for inhibition of protein translation) were determined, with GAPDH (37 kDa) as loading control. Data information: **(A, D, I)** RT-qPCRs were analyzed using qBase-plus with *SDHA*, *RPL13A* and *YWHAZ* serving as reference genes. Note that the mRNA levels of the targets of interest are normalized to those of the above-mentioned reference genes (relative mRNA expression in the y-axis). The scatter plots represent the mean (solid line) \pm SEM. Statistical analyses were performed using GraphPad Prism 9, using a one-way ANOVA with post-hoc testing. **(B, E, F, G, J)** One representative image is shown for each WB experiment, with the number of biological replicates mentioned in each panel description

(positive control: LC-3) or via proteasomal degradation, as evaluated with the proteasome inhibitor MG132 (positive control: Hsp70) (Supplementary Fig.S2B–E).

Taken together, GCs decrease both MR mRNA and protein levels in MM cell lines with different degrees of GC-mediated MM cell killing in a GR-dependent manner, corroborating the existence of GR-MR crosstalk in these cells (Fig. 1H). Our findings also demonstrate that MR mRNA is unstable and that Dex requires de novo transcription and translation to decrease MR levels in MM cells.

MR antagonism enhances GC responsiveness of MM1.S cells

Because Dex can decrease MR mRNA and protein levels in MM cells, we examined whether a targeting of MR could affect the anti-MM activity of GCs. Hereto, we used three different strategies. First, we used MR knockdown using siRNA's (siMR, Fig. 2A, B) and found that the MM1.S cell viability was markedly reduced even in the absence of Dex (Fig. 2A). Although the effect size by which Dex reduced the MM1.S cell viability was comparable in siCtrl and siMR conditions, the cell viability was significantly lower ($\sim 55\%$) in the siMR Dex compared to the siCtrl Dex condition ($\sim 80\%$, Fig. 2A). Altogether, this suggests that MR presence may protect against myeloma cell death.

Second, to evaluate how MR levels evolve upon prolonged GC treatment, we developed a cell model that mimics the gradual build-up of GC resistance. Here, MM1.S cells were treated for four weeks with a low dose of Dex (10^{-8} M) followed by a high dose of Dex (10^{-6} M) for 24 h to assess the residual GC responsiveness of the MM cells to cell killing (Fig. 2C). When MM cells were treated for four weeks with solvent, the additional 24 h high-dose Dex resulted in a marked decrease in MR protein levels (Fig. 2C, lane 1 vs 2), in line with Fig. 1B. In contrast, after four weeks low-dose Dex, MR levels no longer declined following a 24 h high-dose Dex (Fig. 2C, lane 3 vs 4). Apoptotic marker analyses confirmed that the four weeks low-dose Dex, indeed rendered MM1.S cells refractory to the 24 h high-dose Dex boost (Fig. 2C, lane 2 vs 4). We found decreased cleavage of pro-apoptotic PARP and caspase 3, reduced levels of pro-apoptotic Bim and increased levels of anti-apoptotic Bcl-XL (Fig. 2C, lane 2 vs 4).

Third, because MR knockdown promoted MM1.S cell killing (Fig. 2A), we sought to complement these findings by using the MR antagonist spironolactone (Spi). A concentration–response experiment showed that 10^{-5} M Spi (24 h) supported minor cell killing in MM1.S cells (Fig. 2D), but not in endothelial MR-positive EA.hy926 cells (72 h, toxicity control, Supplementary Fig.S3A). Next, we treated MM1.S cells for 24 h with a combination of Dex (10^{-6} M) and Spi (10^{-5} M) and showed increased cleavage of pro-apoptotic PARP and caspase 3, and a decrease in anti-apoptotic Bcl-xL (Fig. 2E). Confirmatory Annexin V/PI flow cytometric analyses showed that Dex-Spi combination decreased the percentage of viable MM1.S cells and increased the percentage of early- and late-apoptotic cells compared to each treatment alone (Fig. 2F, G Supplementary Fig.S3B). Spi enhanced Dex-induced MM1.S cell killing already at 24 h (Fig. 2H) and at 72 h to an even higher extent (Fig. 2I). Finally, also Pred- and Hcort-mediated MM1.S cell killing was boosted by Spi (Fig. 2J, K).

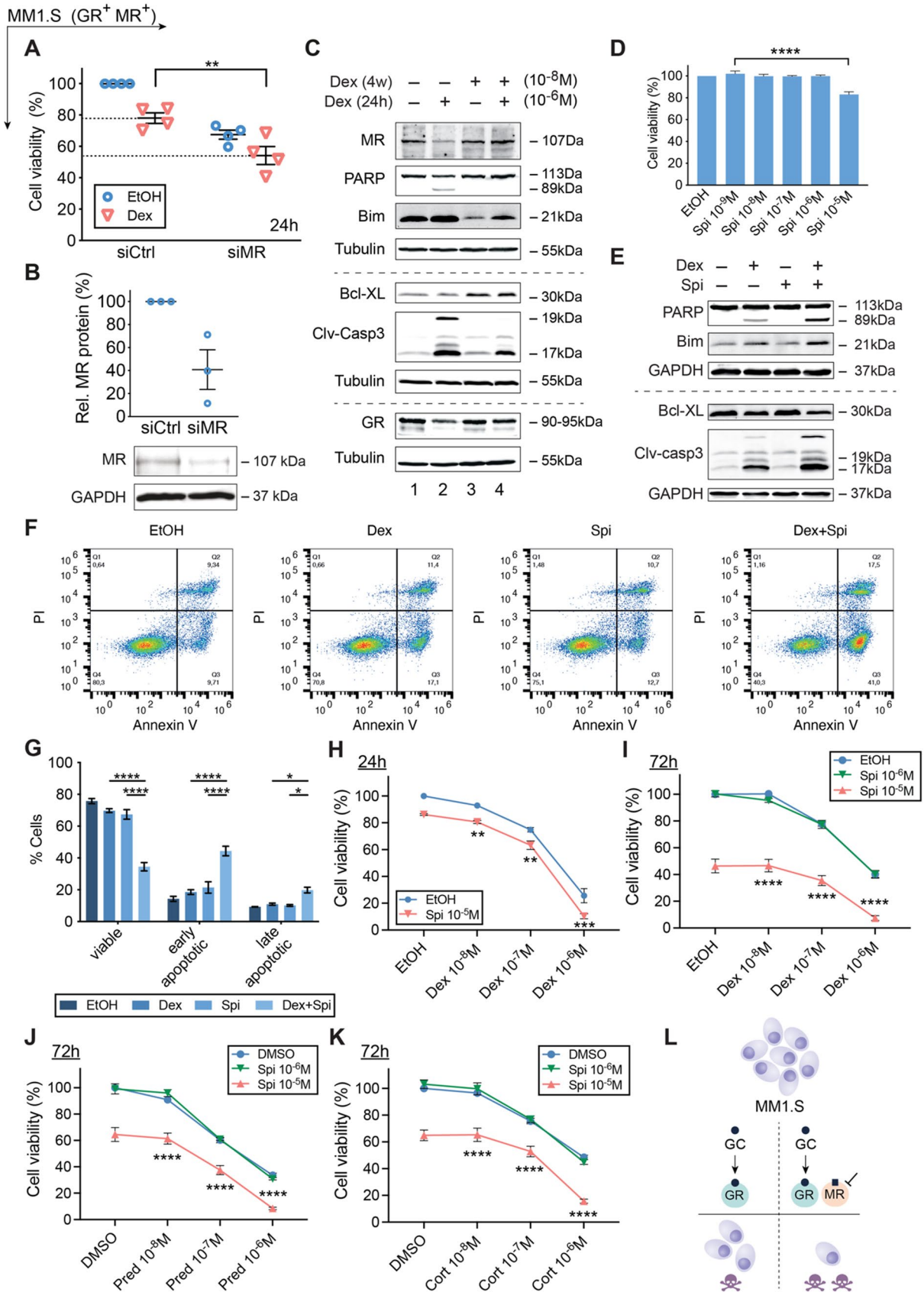


Fig. 2 GC-induced MM1.S cell killing is promoted by the MR antagonist Spi. **(A)** MM1.S cells were nucleofected with siCtrl (scrambled) or siMR. 48 h post-nucleofection, cells were reseeded and treated for another 24 h with Dex (10^{-6} M) or solvent control (EtOH), followed by a CelltiterGlo assay. The scatter plot represents the mean (solid line) \pm SEM ($N=4$). The siCtrl solvent condition was set as 100% and the other conditions were recalculated accordingly. **(B)** 72 h post-nucleofection with siCtrl or siMR, WB analyses were performed and MR protein levels relative to GAPDH were quantified by band densitometric analysis using ImageJ. The scatter plot represents the mean \pm SEM ($N=3$). **(C)** MM1.S cells were treated for 4 weeks with 10^{-8} M Dex (or EtOH), followed by 24 h 10^{-6} M Dex (or EtOH), and subjected to WB analyses ($N=3$). **(D)** MM1.S cells were treated with a Spi concentration range (10^{-5} M– 10^{-9} M) or solvent control (set as 100%), followed by a CelltiterGlo assay ($N=3$). **(E–G)** MM1.S cells were treated with Dex (10^{-6} M), Spi (10^{-5} M) or a Dex-Spi combination for 24 h, followed by **(E)** WB analyses ($N=4$) or **(F, G)** Annexin V/PI flow cytometric analyses ($N=4$). **(F)** Representative quadrant plots of 4 independent experiments for each treatment condition, with **(G)** bar plots showing the percentage of viable (Q4), early apoptotic (Q3), late apoptotic (Q2) averaged over all 4 biological repetitions \pm SEM. **(H, I)** MM1.S cells were treated with Dex (10^{-6} M– 10^{-8} M), Spi (10^{-5} – 10^{-6} M) or a Dex-Spi combination for **(H)** 24 h ($N=5$) or **(I)** 72 h ($N=3$), followed by a CelltiterGlo assay (solvent control set as 100%). **(J, K)** MM1.S cells were treated with Pred or Cort (10^{-6} M– 10^{-8} M), Spi (10^{-5} – 10^{-6} M) or a Pred/Spi or Cort/Spi combination for 72 h ($N=3$), followed by a CelltiterGlo assay (solvent control set as 100%). **(L)** Summarizing model demonstrating that MR blockade increases Dex-induced MM1.S cell killing. Data information: **(A, D, G–K)** Statistical analyses were performed using GraphPad Prism 9, using **(A, D)** one-way or **(G–K)** two-way ANOVA with post hoc testing. **(C, E)** Protein lysates were subjected to WB analyses, visualizing the protein levels of MR (107 kDa), GR (90–95 kDa), PARP (89 and 113 kDa), Bim (21 kDa), Bcl-XL (30 kDa) and cleaved-caspase 3 (17 and 19 kDa). Tubulin (55 kDa) or GAPDH (37 kDa) served as loading controls. One representative image is shown for each WB experiment, with the number of biological replicates mentioned in each panel description

Summarized, our results suggest that MR is a pro-survival factor in myeloma and that its pharmacological inhibition enhances GC-induced MM1.S cell killing.

The ability of Spi to promote Dex-induced cell killing correlates with the Dex responsiveness of MM cell lines

To determine whether a Dex-Spi combination is effective across MM cell line models, we screened four other MM cell lines in which GCs induce MM cell killing to varying extents (Fig. 1C). Whereas the MR antagonist Spi did not readily promote GC-mediated OPM-2 killing at 24 h of treatment, this was observed after 72 h of treatment (Fig. 3A) as strongly as in MM1.S cells (Fig. 2I). Hence, the threshold to obtain an efficient Dex-Spi-induced killing could have a time-dependent component when comparing OPM-2 to MM1.S.

Next, we tested MM cells that are less (or un)responsive to Dex in terms of cell killing to evaluate whether Dex-Spi still offers therapeutic benefit. Although L-363 cells respond

slightly to Dex treatment, Spi did not significantly impact Dex-mediated cell killing of these cells after 72 h (Fig. 3B), which may be due to the very low amounts of MR that these cells contain (only detectable at mRNA level, Fig. 1A, B). The same reasoning applies to the Dex-unresponsive U-266 cells, where Spi alone caused only a minor drop in cell viability ($\sim 10\%$, Fig. 3C). Interestingly, in MM1.R cells, which are GR-negative yet strongly MR-positive (Fig. 1B), Spi alone triggered a marked decrease in cell viability at 72 h of treatment (drop of $\sim 30\%$, Fig. 3D), for which GR presence is clearly not required.

In summary, in myeloma cells that contain detectable protein levels of both GR and MR, Spi enhances Dex-induced myeloma cell killing (Fig. 3E).

Combining lower doses of GC with MR antagonist enhances cell death of primary MM cells

To validate the potential of a Dex-Spi combination treatment in a preclinical context, we isolated primary MM cells from bone marrow aspirates of 10 MM patients at different disease stages (Table 1). In line with our observations in MM1.S and OPM-2 cells, newly diagnosed MM1 (Fig. 4A) and MM2 (Fig. 4B) patient cells as well as the premalignant smoldering MM9 patient cells (Fig. 4K) displayed higher cell killing when combining Dex and Spi versus Dex alone. Importantly, 10^{-7} M Dex combined with 10^{-5} M Spi was at least equally efficacious as 10^{-6} M Dex (~ 40 mg comparator dose in patients) alone (full arrow). As could be expected from a heterogeneous disease as myeloma, not all patient samples responded alike. Newly diagnosed MM3 patient cells (Fig. 4C) strongly responded to Dex but had no additional benefit from Spi treatment. Furthermore, MM10 cells of a premalignant MGUS patient (Fig. 4L) hardly responded to Dex treatment, while Spi alone reduced the cell viability with about 20% (dashed arrow). Notable, in all relapsed patient cells (MM4, MM5, MM6, MM7 and MM8, Fig. 4D–H), Spi alone triggered a pronounced cell killing (Fig. 4D–H), with a reduced cell viability of max. up to 60% (Fig. 4H). All relapsed patient cells were found to be resistant to Dex-induced cell killing, except MM4, which may explain why a Dex-Spi combination did not further improve on cell killing as compared to Spi alone.

Only for MM1, MM2, MM3, MM4 and MM5 patients the primary cell yield was sufficiently high to allow for an analysis of GR and MR target gene expression following Dex treatment. We selected *TSC22D3* and *SGK1* because (1) of their opposing Dex response in our MM cell lines (Supplementary Fig.S1), (2); studies indicate anti-proliferative actions (*TSC22D3*) [39] or pro-survival effects (*SGK1*) [41], and (3); the receptors themselves were below the detection limit as assessed by RT-qPCR. Dex treatment upregulated *TSC22D3* mRNA levels in 2 out of 3 newly diagnosed

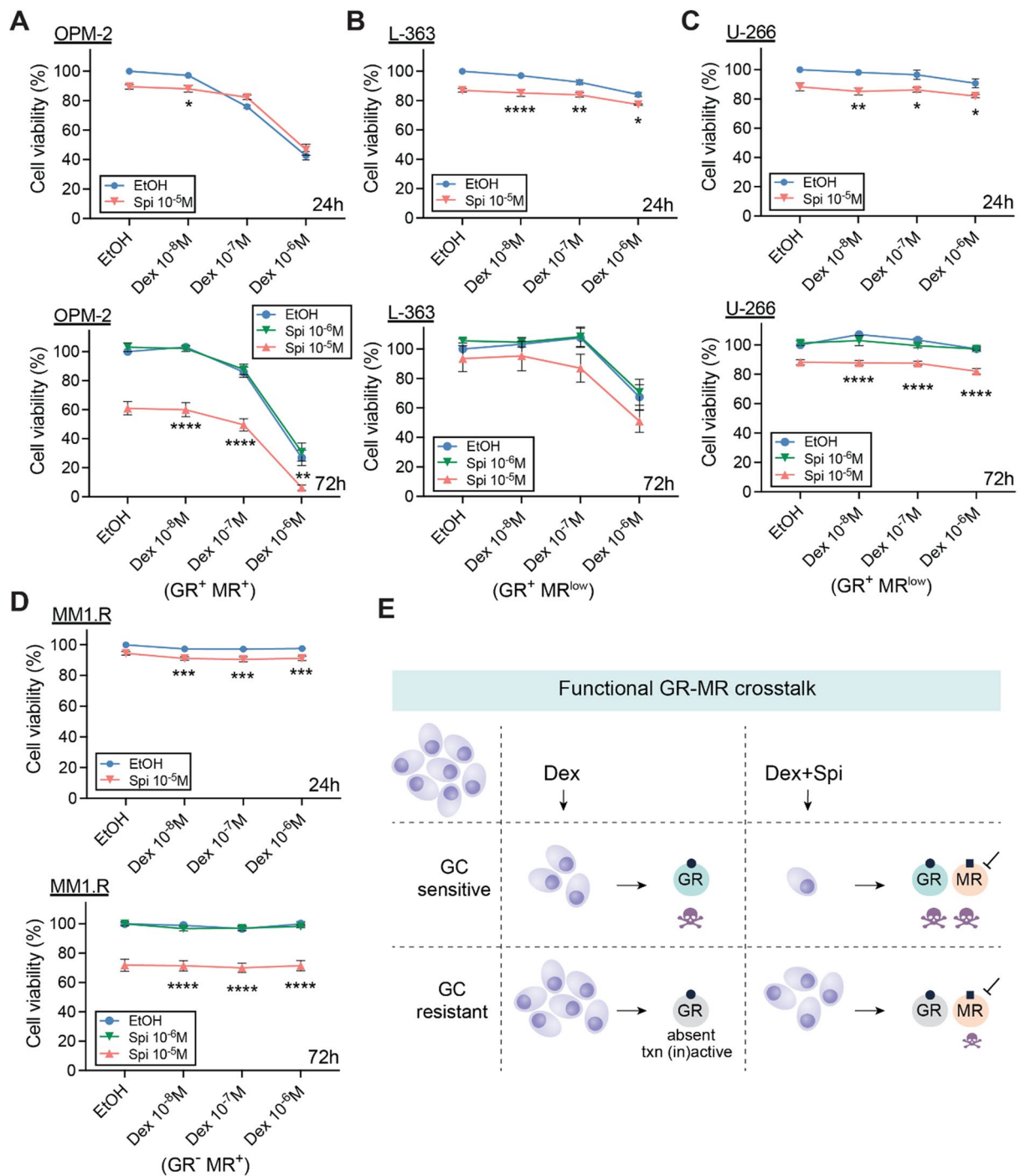


Fig. 3 The MR antagonist Spi promotes cell killing of MM cells with varying degrees of Dex responsiveness. (**A–D**) Different myeloma cell lines including (**A**) OPM-2, (**B**) L-363, (**C**) U-266 and (**D**) MM1.R cells were treated with Dex (10^{-6} M– 10^{-8} M), Spi (10^{-5} – 10^{-6} M), a Dex-Spi combination or solvent control (set as 100%) for 24 h or 72 h, followed by a CelltiterGlo assay. Biological replicates: OPM-2 (24 h $N=6$; 72 h $N=4$), L-363 (24 h and 72 h $N=3$), U-266 (24 h $N=4$, 72 h $N=3$) and MM1.R (24 h $N=4$, 72 h

$N=3$). (**E**) Graphical summary highlighting the existence of a functional crosstalk between GR and MR in MM cells. In GC-sensitive MM cells containing GR, Dex induces MM cell killing, which is further enhanced by the addition of Spi. In GC-resistant cells, where GR is either absent or transcriptionally (inactive), Dex loses its anti-MM activity, while Spi addition does trigger significant MM cell killing. Data information: (**A–D**) Statistical analyses were performed using GraphPad Prism 9 using two-way ANOVA with post hoc testing

Table 1 Patient demographics and disease stage

Pseudonym	Gender	Age	Stage	M protein type
MM1	F	60	Newly diagnosed, prior to first therapy	IgG κ
MM2	F	69	Newly diagnosed, prior to first therapy	IgG κ
MM3	M	64	Newly diagnosed, prior to first therapy	κ light chain
MM4	F	71	Relapsed, prior to start of 6th line therapy	IgG λ
MM5	M	66	Relapsed, prior to start of 6th line therapy	λ light chain
MM6	M	64	Relapsed, prior to 2nd line of therapy	IgG κ
MM7	F	71	Relapsed, prior to 2nd line of therapy	κ light chain
MM8	M	56	Relapsed, prior to 2nd line of therapy	IgA κ
MM9	F	31	High-risk SMM	IgG λ
MM10	M	53	MGUS	IgM κ

MGUS monoclonal gammopathy of undetermined significance, SMM smoldering multiple myeloma

patient cells (MM1 and MM3) and in both relapsed patient cells (MM4 and MM5) (Fig. 4I), while SGK1 mRNA levels were downregulated in 1 out of 3 newly diagnosed patient cells (MM3) and in both relapsed patient cells (MM4 and MM5) (Fig. 4J); hereby recapitulating the varying degree in Dex-responsiveness that was also retrieved in the MM cell lines (Supplementary Fig.S1).

To examine whether *NR3C2* and/or *NR3C1* expression levels could predict survival, we took advantage of publicly available RNA-sequencing data generated in the framework of the CoMMpass study of the MM research foundation (MMRF). We found that *NR3C2* levels were much lower than those of *NR3C1* at diagnosis (Fig. 4N). Nonetheless, *NR3C2* levels were predictive for overall survival (OS) when patients were divided into 3 groups based on high, medium, and low expression of *NR3C2* (Fig. 4O). This was not the case when progression-free survival (PFS) was assessed (Supplementary Fig.S4A). *NR3C1* expression levels were not predictive of either PFS or OS (Fig. 4P, Supplementary Fig. 4B).

Taken together, in newly diagnosed and premalignant myeloma patients, a tenfold lower Dex dose in combination with Spi could be advantageous, although the extent of the therapeutic benefit will differ among patients (Fig. 4M, top panel). In the relapsed setting, Dex is barely functional, but Spi alone does induce distinct MM cell killing (Fig. 4M, bottom panel). Finally, *NR3C2*, but not *NR3C1* expression levels are associated with OS in patients.

GR and MR interact at the endogenous level in MM cells

Because crosstalk mechanisms between nuclear receptors can arise from a direct interaction [13], we examined to which extent and in which direction Dex-Spi steers GR–MR heterodimerization compared to Dex, via two complementary methods. First, we developed a NanoBiT-based quantitative GR–MR heterodimerization assay in HEK293T cells

that relies on overexpressed tagged receptors and *in cellulo* reconstitution of a functional NanoLuc luciferase (Fig. 5A). In this assay, a signal for GR–MR heterodimerization is only measured when GR coupled to SmBiT (at C-terminus) and LgBiT coupled to MR (at N-terminus) interact (Fig. 5A). The NanoBiT assay is, however, not discriminative in pinpointing the interaction to a specific subcellular location. We found that Dex triggered an ~eightfold induction of GR–MR heterodimerization, which was reduced when combined with Spi to ~sixfold (Fig. 5B, C). In contrast, Spi alone failed to induce GR–MR heterodimerization.

We compared the NanoBiT assay results with endogenous GR–MR co-immunoprecipitation (co-IP) analyses in MM1.S and OPM-2 cells. Already in basal conditions, GR and MR interacted in the IP fraction (lane 2, Fig. 5D, F). In line with the NanoBiT results, Dex treatment consistently increased this interaction in MM1.S and OPM-2 cells. Similarly, Dex-Spi combination again reduced this GR–MR interaction compared to Dex treatment. In contrast to NanoBiT, Spi alone did support a marked GR–MR interaction in an endogenous context, although to a lower extent than Dex alone.

To examine whether the Dex-Spi combination could also impact receptor homodimer formation, we extended our NanoBiT assay portfolio toward GR–GR and MR–MR homodimerization. We found that Dex triggered a ~3.5-fold induction in GR–GR homodimer formation, which was unaffected by the addition of Spi (Fig. 5H, I). In contrast, Spi completely abolished the Dex-induced MR–MR homodimer formation (Fig. 5J, K).

Summarized, GR and MR engage in an endogenous interaction in MM cells. Quantitative assays indicate that Spi blunts Dex-induced GR–MR and MR–MR dimerization.

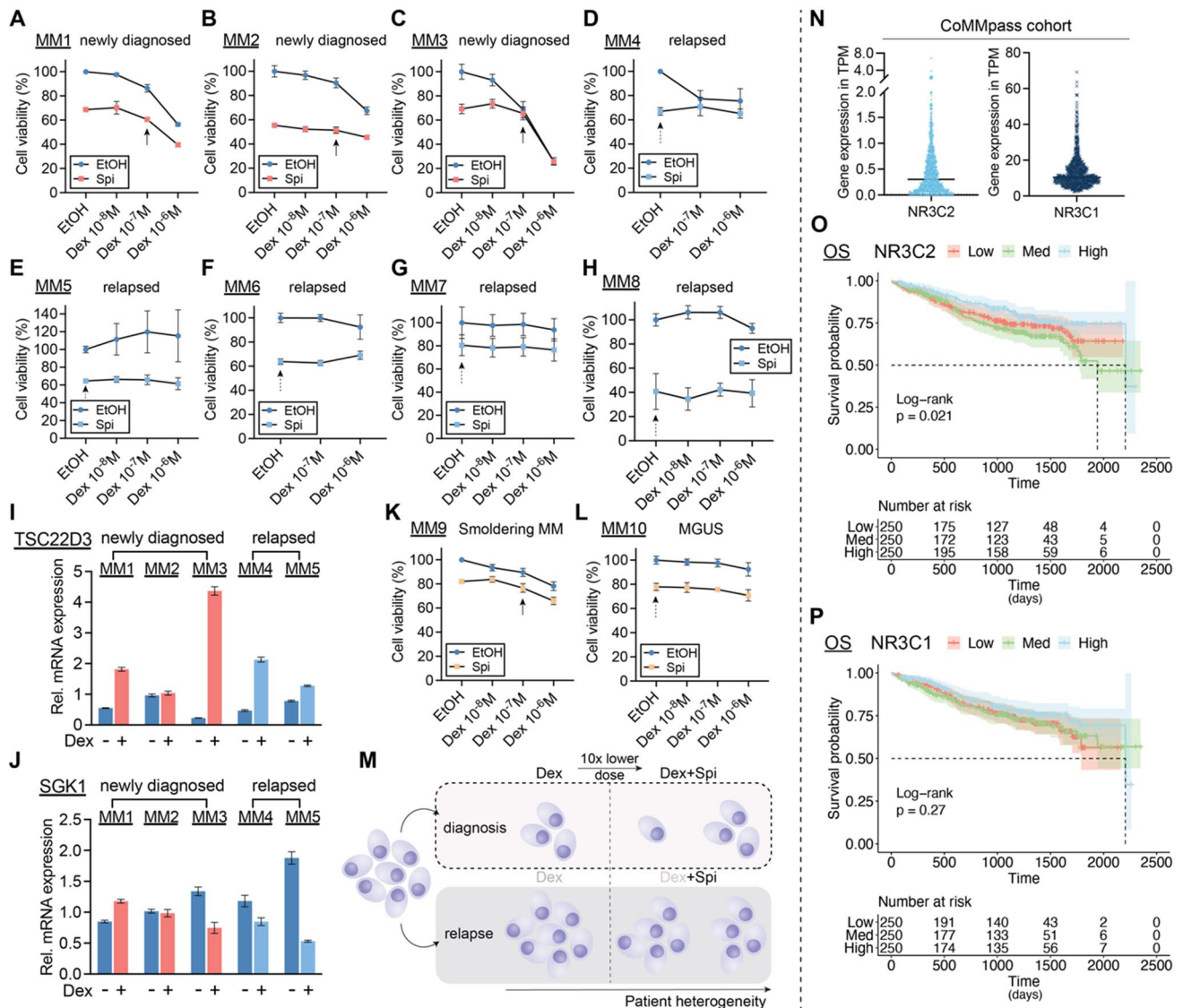


Fig. 4 Combining lower doses of Dex with the MR antagonist Spi enhances cell killing in primary myeloma cells depending on the disease stage. (**A–H**) Patient-derived MM cells from bone marrow aspirates of (**A–C**) newly diagnosed, (**D–H**) relapsed or MM patients were treated with a Dex concentration range (10^{-6} M– 10^{-8} M), Spi (10^{-5} M), a Dex-Spi combination or solvent control (EtOH) for 24 h (**A, C–G**) or 72 h (**B, H**), followed by a CelltiterGlo cell viability assay. (**I, J**) When the primary cell yield was sufficient, primary MM cells were treated for 6 h with Dex (10^{-6} M) or solvent control, followed by RNA isolation and RT-qPCR analyses to determine the expression levels of *TSC22D3* (GILZ) and *SGK1*. Data analyses were performed using qBaseplus with *SDHA*, *RPL13A* and *YWHAZ* serving as reference genes. Note that the mRNA levels of the targets of interest are normalized to those of the above-mentioned reference genes (relative mRNA expression in the y-axis). The bar plots represent the mean \pm SD of 3 technical replicates. Overall, no statistical analyses were performed because only 1 biological replicate could be carried out given the limited culturing time of primary MM cells isolated from a BM aspirate. (**K, L**) Patient-derived MM cells from bone marrow aspirates of premalignant (smoldering MM or MGUS) myeloma patients were treated with a Dex concentration range (10^{-6} M– 10^{-8} M), Spi (10^{-5} M), a Dex-Spi combination or solvent control (EtOH) for 24 h (**L**) or 48 h (**K**) followed by a CelltiterGlo

cell viability assay. (**M**) Graphical summary demonstrating that primary MM cells isolated at diagnosis undergo profound Dex-mediated cell killing, while the addition of Spi to a tenfold lower Dex dose triggers more extensive cell killing, although not the same extent in all patients. In the relapsed setting, Dex is unable to induce significant primary MM cell killing, while Spi triggers a substantial MM cell killing response. The extent of the described cell killing effects varies from patient to patient, due to interpatient heterogeneity, which is well known in MM. (**N**) TPM (transcripts per million) gene expression values, generated via RNA-sequencing, of *NR3C2* (MR) and *NR3C1* (GR) in the CoMMpass cohort; only samples at diagnosis were taken along. (**O, P**) Kaplan–Meier curve of the MMRF patient cohort, depicting the survival probability in function of overall survival (OS) for low, medium or high expression of (**O**) *NR3C2* or (**P**) *NR3C1*. Statistical analyses were performed in R (package survival), using a log-rank test. Data information: (**A–H, K, L**) Each data point represents the mean \pm SD of technical replicates because only one biological repetition could be performed with the primary myeloma cells. The solvent condition was set as 100% and the other conditions were recalculated accordingly. Full arrows highlight the effect of the combination of a tenfold lower Dex dose with Spi, while dashed arrows indicate the effect of Spi alone

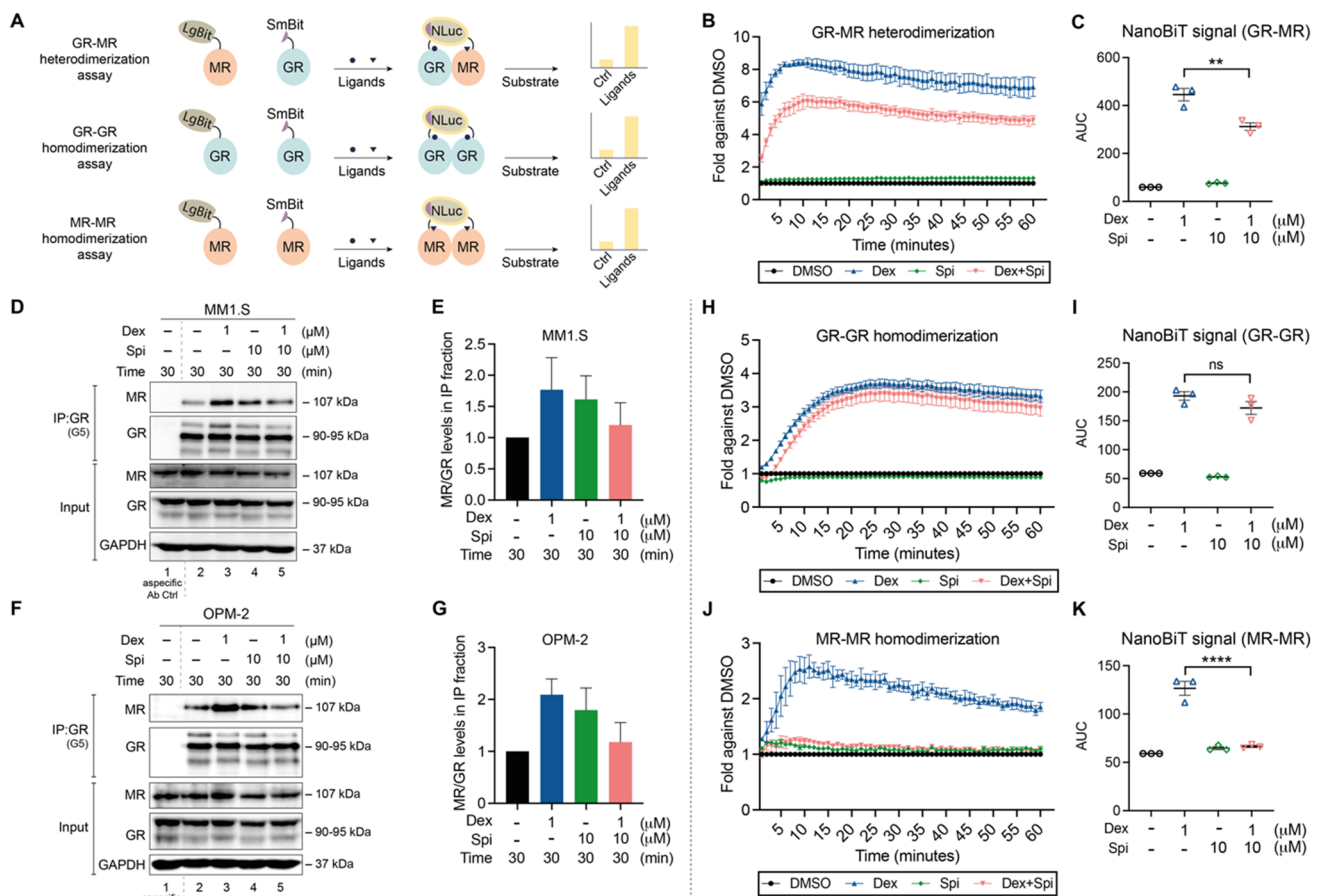


Fig. 5 Crosstalk between GR and MR may result from an endogenous interaction that can be modulated with ligands. **(A)** Principle of the NanoBiT-based dimerization assays. In the GR–MR heterodimerization assay, the Large BiT (LgBiT) and Small BiT (SmBiT) fragments of the NanoLuc® luciferase, which have very low affinity for each other, are coupled to MR (at the N-terminus) or GR (at the C-terminus), respectively, and transfected into HEK293T cells. When the addition of ligand promotes GR–MR heterodimerization, the LgBiT and SmBiT come in close proximity of each other, hereby reconstituting the functional NanoLuc® luciferase. Following substrate addition (furimazine, cell-permeable substrate), the bioluminescent signal can be measured in intact cells. This NanoBiT-based assay was expanded to also measure GR–GR and MR–MR homodimerization. In both cases, LgBiT was coupled to the N-terminus and SmBiT to the C-terminus of both respective receptors. **(B, C)** HEK293T cells were transfected with LgBiT–MR and GR–SmBiT. 24 h post-transfection, substrate is added and the baseline luminescence is recorded. Thereafter, cells are treated with Dex (10^{-6} M), Spi (10^{-5} M), the combination thereof, or solvent control and luminescence is measured continuous during 60 min (1-min intervals) ($N=3$). **(C)** Statistical comparison of the area under the curve of Dex vs Dex–Spi NanoBiT results in panel **B** ($N=3$). **(D–G)** Two myeloma

cell lines, i.e. **(D)** MM1.S and **(F)** OPM-2 cells were treated with Dex (10^{-6} M), Spi (10^{-5} M), a Dex–Spi combination or solvent control for 30 min. Protein lysates were prepared and subjected to endogenous immunoprecipitation using GR (G5) antibody (both cell lines $N=2$). Thereafter, WB analyses were performed to determine co-immunoprecipitation of GR (90–95 kDa) with MR (107 kDa). GAPDH served as loading control for the input fraction. Lane 1 represents the non-specific antibody control. **(E, G)** In the IP fraction, MR protein levels were quantified relative to GR protein levels by band densitometric analysis using ImageJ. The bar plot displays the ratio of MR/GR in the IP fraction averaged over both biological repetitions (+/SEM). **(H–K)** HEK293T cells were transfected with **(H)** LgBiT–GR and GR–SmBiT, or **(J)** LgBiT–MR and MR–SmBiT. 24 h post-transfection, substrate is added and the baseline luminescence is recorded. Thereafter, cells are treated with Dex (10^{-6} M), Spi (10^{-5} M), the combination thereof, or solvent control and luminescence is measured continuous during 60 min (1-min intervals) ($N=3$). **(I, K)** Statistical comparison of the area under the curve of Dex vs Dex–Spi NanoBiT results in panel **H** and **J** ($N=3$). Data information: **(D, F)** One representative image is shown for each co-IP experiment; the other biological replicates are available for consultation in Supplementary Fig. 5

Dex–Spi combination strongly inhibits several major players in myeloma cell survival

To determine whether GR–MR crosstalk leads to differential transcriptomic signatures, we followed an RNA-sequencing

approach. Principal component analysis showed that the biological repeats are clustered well by condition (EtOH, Dex, Spi, Dex–Spi) (Supplementary Fig.S6A). Differential gene expression analysis of pairwise comparisons revealed that the highest number of unique genes were regulated by

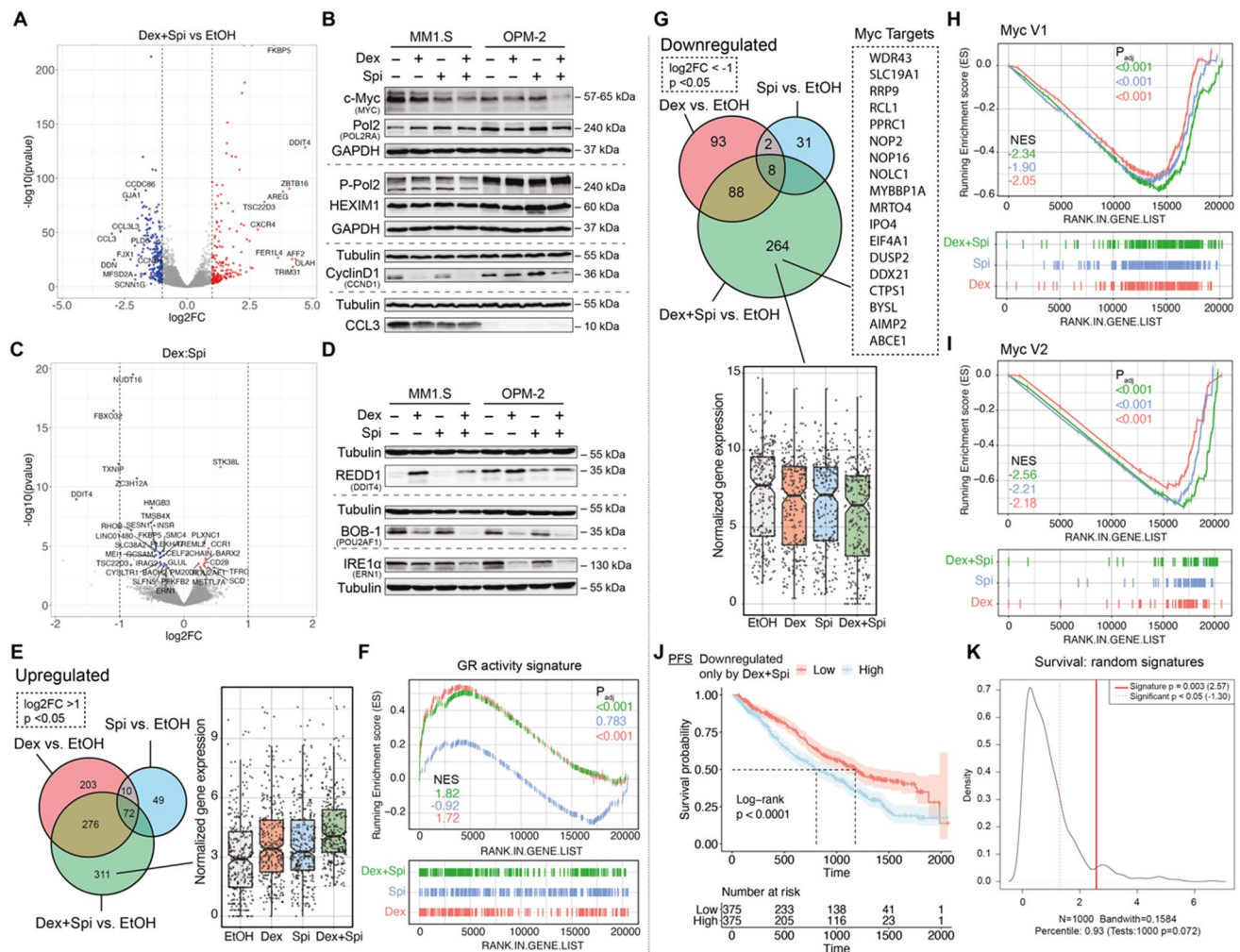


Fig. 6 c-myc and its target genes are inhibited most by Dex-Spi treatment, while a subset of Dex-Spi downregulated genes may predict prognosis. **(A, C)** MM1.S cells were treated with Dex (10^{-6} M), Spi (10^{-5} M), a Dex-Spi combination or solvent control (EtOH) for 6 h, followed by RNA-seq analysis. **(A, C)** Volcano plots depicting the p_{adj} (log₁₀ scale) in function of the log₂FC for all genes with base-Mean ≥ 50 for **(A)** the pairwise comparison Dex-Spi vs EtOH or **(C)** the interaction term genes (=those for which the response following Dex-Spi treatment is significantly different from combining the separate responses of Dex and Spi). Significantly regulated genes ($p_{\text{adj}} < 0.05$) are colored in red (log₂FC > 1 in **A**, log₂FC > 0 for **C**, upregulated) or blue (log₂FC < -1 in **A**, log₂FC < 0 for **C**, downregulated); non-significant genes ($p_{\text{adj}} > 0.05$) in grey. The gene names are displayed for those genes having the largest abs(log₂FC) values (top 10 upregulated/downregulated). The dashed lines are set at abs(log₂FC) = 1. **(B, D)** MM1.S and OPM-2 cells were treated with Dex (10^{-6} M), Spi (10^{-5} M), a Dex-Spi combination or solvent control (EtOH) for 24 h (both $N = 3$). Protein lysates were prepared and subjected to WB analyses, hereby assessing the protein levels of (P-Ser2) Pol2 (240 kDa), GR (90–95 kDa), c-myc (57–65 kDa), cyclin D1 (36 kDa), MIP-1 α (CCL3, 10 kDa), DDIT4 (35 kDa), IRE1 α (110–130 kDa) and BOB-1 (35 kDa). GAPDH (37 kDa) and Tubulin

(55 kDa) served as loading controls. **(E, G)** Venn diagram of three pairwise comparisons, split up in genes that were either **(E)** upregulated or **(G)** downregulated. In addition, the normalized gene expression profiles of the genes that are uniquely regulated by Dex-Spi are shown. **(F, H, I)** Gene set enrichment analysis (GSEA) of single hallmarks, i.e. **(F)** a GR activity signature and **(H, I)** two sets of cyc target genes (V1, V2), for each pairwise comparison, along with the respective normalized enrichment score (NES) and p_{adj} . **(J)** Kaplan-Meier curve of the MMRF patient cohort ($N = 750$), depicting the survival probability in function of progression-free survival (PFS) for low or high expression of genes that were uniquely downregulated by the Dex-Spi combination. Statistical analyses were performed in R (package survival), using a log-rank test. **(K)** Prognostic factor analysis of the genes uniquely downregulated Dex-Spi (red solid curve) versus random signatures (red dotted curve). Prognostic power as determined by SigCheck (R package) of the genes uniquely downregulated by Dex-Spi (red dotted line) with 1000 random gene-sets of the same size (P value < 0.05 is indicated by the red dotted line) for the PFS parameter in the CoMMpass cohort. Data information: **(B, D)** One representative image is shown for each WB experiment, with the number of biological replicates mentioned in each panel description

Dex-Spi (596) (Supplementary Fig.S6B). Volcano plots further highlight significant genes with the largest log₂ fold changes (log₂FC; red and blue) for different pairwise comparisons, including ‘Dex-Spi vs EtOH’ (Fig. 6A), ‘Dex vs EtOH’ and ‘Spi vs EtOH’ (Supplementary Fig.S6C). Several top genes that were shared between pairwise comparisons and that are typical target genes for GR and MR, i.e., *TSC22D3*, *FKBP5* and *SGK1*, were analyzed by RT-qPCR to validate the RNA-sequencing results (Supplementary Fig. S6B). In MM1.S, OPM-2 and L-363 cells, *TSC22D3* (anti-proliferative action) [39] and *FKBP5* (GR co-chaperone) [42] mRNA levels were upregulated to a lesser extent by 6 h Dex-Spi treatment than by Dex alone, in line with their corresponding count plots (Supplementary Fig.S6D-H). In addition, *SGK1* (stimulates myeloma cell survival) [41] mRNA levels were downregulated to a similar extent by Dex-Spi and Dex in MM1.S and L-363 cells, again in line with the RNA-sequencing results. In search of significantly regulated side-effect markers, the bone homeostasis marker *TMEM119* [43, 44] was selected, given that this gene may act as a molecular proxy for GC-related bone disease. Dex-Spi combination showed a mild, yet consistent upregulation of *TMEM119* in MM1.S, OPM-2 and L-363 cells (Supplementary Fig.S6D-H).

To prioritize candidate genes for validation at the protein level, we identified the molecular and cellular functions attributable to the ‘Dex-Spi vs EtOH’ comparison by performing an Ingenuity Pathway Analysis (IPA). We found groups of genes that were significantly involved in gene transcription (terms: gene expression and RNA post-transcriptional modification), cell death and survival and cell cycle (Supplementary Fig.S7A). Based on the top regulated genes from each comparison in these IPA terms (Fig. 6A, Supplementary Fig.S6C, S7A), we selected genes that were involved in transcriptional regulation (*POLR2A*, *HEXIM1*), cell growth, proliferation and/or survival (*MYC*, *CCND1*, *CCL3*) and validated these at the protein level in MM1.S, OPM-2, L-363 and MM1.R cells (Fig. 6B, Supplementary Fig.S7B-C). Interestingly, c-myc (oncogene) [45] protein levels were significantly decreased by Dex-Spi as compared to Dex alone in both MM1.S and OPM-2 cells (Fig. 6B), again in line with our RNA-sequencing results, and also by Spi alone in MM1.R cells (Supplementary Fig.S7C). Whereas RNA polymerase 2 (Pol 2) levels were largely unchanged comparing Dex-Spi versus Dex alone, activated Pol 2 protein levels, hallmarked by Ser2 phosphorylation [46], decreased markedly upon Dex-Spi, yet only in MM1.S cells (Fig. 6B), indicating a halt in the transcription elongation process. In OPM-2 cells, a brake on transcription induced by Dex-Spi may rather originate from a mild upregulation (vs Dex) of the transcriptional repressor *HEXIM1* [47]. Cyclin D1, a protein downregulated by GCs to induce cell cycle arrest [48], was downregulated to the

same extent by Dex-Spi as by Dex alone in MM1.S cells, while in OPM-2 cells, Dex-Spi triggered the largest decrease in cyclin D1 protein levels. In addition, in MM1.S cells, the protein levels of *CCL3*, a contributor to myeloma cell migration and an aggravator of bone disease [49], were decreased similarly in all conditions versus solvent (Fig. 7B). In OPM-2 and L-363 cells, *CCL3* was largely undetectable.

We also examined the Dex:Spi interaction term (Fig. 6C), which contained 37 significantly regulated genes (Supplementary Table S5) and of which the response following Dex-Spi treatment is hypothesized to be significantly different from combining the responses of separate Dex and Spi treatments. Three genes were selected for validation at the protein level based on their high normalized counts, previously described function in myeloma, and accompanying primary antibody performance (in WB): (1) *DDIT4* (also known as REDD-1), promotes myeloma cell growth and survival [50] and is described as a GC-inducible muscle atrophy marker [51]; (2) *ERN1* (also known as IRE1 α), a sensor of unfolded proteins and critical for MM tumor growth [52]; (3) *POU2AF1* (also known as BOB-1), a regulator of oncogenic networks in myeloma [53]. Interestingly, REDD1 protein levels were decreased by Dex-Spi combination versus Dex in MM1.S cells and, to a similar extent, by Spi and Dex-Spi in OPM-2 cells (Fig. 6D). In L-363 cells, REDD1 levels were equally increased by Dex and Dex-Spi (Supplementary Fig. S7D). Both BOB-1 and IRE1 α were most strongly decreased by Dex-Spi combination in MM1.S cells and comparably decreased by Dex and Dex-Spi treatment in OPM-2 cells (Fig. 6D). In L-363 and MM1.R cells, IRE1 α levels were not clearly regulated by any treatment (Supplementary Fig. S7D).

Taken together, our transcriptome analysis and subsequent validation at the protein level reveals that gene transcription is halted more strongly by Dex-Spi than by Dex alone in MM cells, with c-myc, cyclinD1, REDD1 and BOB-1 being strongly Dex-Spi-downregulated targets.

c-myc target genes are mostly downregulated by Dex-Spi

We expanded our RNA-seq analysis by zooming-in on genes that were uniquely up- or down-regulated by the Dex-Spi combination. We found 311 genes to be uniquely upregulated by Dex-Spi, as shown by their normalized gene expression profile (Fig. 6E). GSEA shows that genes upregulated by Dex-Spi (green curve) or Dex (red curve) treatment were enriched for a previously established GR activity score [32] (Fig. 6F).

We then focused on the 264 genes that are uniquely downregulated by Dex-Spi treatment and for which their normalized gene expression is depicted in Fig. 6G. GSEA-based overrepresentation analysis (Supplementary

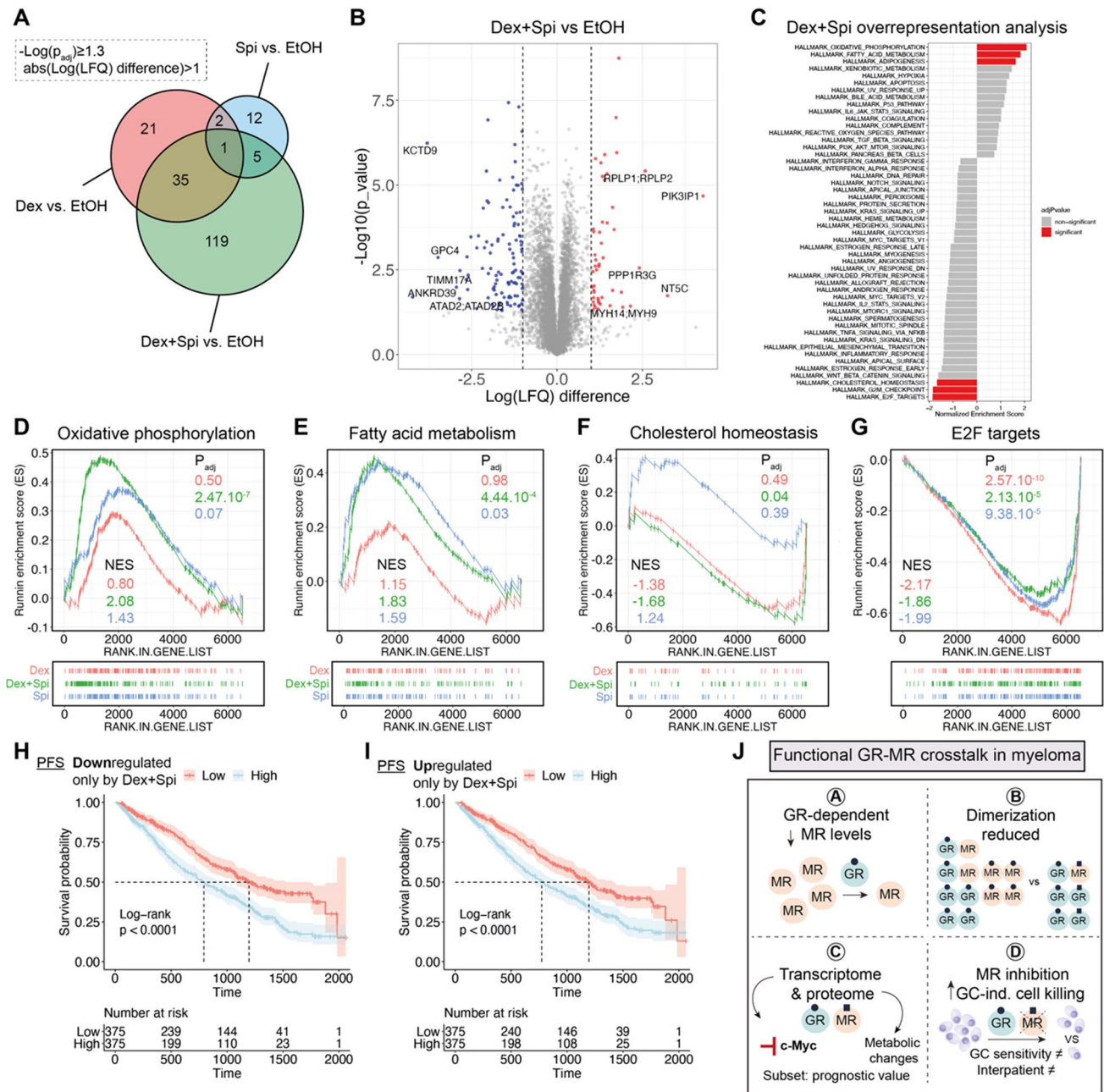


Fig.S7E) identified that two hallmarks containing different sets of myc target genes were significantly enriched in the set of genes that are uniquely downregulated by Dex-Spi. Zooming-in on these ‘myc hallmarks’ (Fig. 6H, I) confirmed that the most negative normalized enrichment scores (NES) were indeed obtained for Dex-Spi. In addition, we examined whether the expression levels of the uniquely Dex-Spi downregulated genes could predict survival, for which we again relied on the CoMMpass cohort data. Strikingly, we found that patients showing low expression of the Dex-Spi downregulated genes had better PFS and OS compared to patients showing high expression

of these genes (Fig. 6J, Supplementary Fig.S7F). Prognostic factor analysis highlighted that this prediction is better than when random gene signatures were used (Fig. 6K, full red line).

Overall, the inhibition of c-myc target genes likely underpins the enhanced myeloma cell killing observed with Dex-Spi.

Fig. 7 Several metabolic pathways are deregulated most by the Dex-Spi combination treatment. (A) MM1.S cells were treated with Dex (10^{-6} M), Spi (10^{-5} M), a Dex-Spi combination or solvent control (EtOH) for 24 h, followed by mass spectrometry-based shotgun proteomics. Venn diagram of pairwise comparisons in which significantly regulated proteins ($-\log(p_{\text{adj}}) \geq 1.3$ with an $\text{abs}(\log(\text{LFQ difference})) > 1$) were considered. (B) Volcano plot depicting the p_{adj} (\log_{10} scale) in function of the $\log(\text{LFQ})$ in the pairwise comparison Dex-Spi vs EtOH. Significantly regulated proteins $-\log(p_{\text{adj}}) \geq 1.3$ are colored in red ($\log(\text{LFQ}) > 1$, upregulated) or blue ($\log(\text{LFQ}) < -1$, downregulated); non-significant genes ($-\log(p_{\text{adj}}) < 1.3$) in grey. (C) GSEA-based overrepresentation analysis for the proteins regulated by Dex-Spi, hereby identifying hallmarks that are significantly (red) or non-significantly (grey) enriched. (D–G) GSEA of single hallmarks, i.e. (D) oxidative phosphorylation, (E) fatty acid metabolism, (F) cholesterol homeostasis or (G) E2F targets, for each pairwise comparison, along with the respective normalized enrichment score (NES) and p_{adj} . (H–I) Kaplan–Meier curves of the MMRF patient cohort ($N=750$), depicting the survival probability in function of progression-free survival (PFS) for low or high expression of proteins that were uniquely (H) downregulated or (I) upregulated by the Dex and Spi combination. Statistical analyses were performed in R (package survival), using a log-rank test. (J) Several lines of evidence support a crosstalk between GR and MR in MM: A) GCs induce a GR-dependent MR downregulation; B) GR and MR engage in a direct, physiologically relevant endogenous interaction that can be modulated by ligands. Spi was shown to reduce the Dex-induced GR–MR heterodimer levels and abolished Dex-induced MR–MR homodimers. Spi did not impact Dex-induced GR–GR homodimerization; C) Dex and Spi combination gives rise to a differential gene and protein expression profile, in which the inhibition of c-myc and its target genes, and several metabolic pathways are modulated most pronouncedly by Dex-Spi, respectively. A specific subset of targets may even have prognostic significance; D) MR inhibition enhances GC-induced cell killing in MM cell lines depending on their GC responsiveness and in primary (heterogeneous) MM cells depending on the disease stage

Shotgun proteomics analyses unveils a contribution of metabolic pathway deregulation upon Dex-Spi treatment

To gain additional mechanistic insights into the Dex-Spi combination treatment at 24-h treatment, we performed mass spectrometry-based shotgun proteomics on MM1.S cells. Differential expression analysis showed that the highest number of hits (i.e. proteins) were again identified for the Dex-Spi combination treatment (Fig. 7A), in line with the RNA-sequencing results (Supplementary Fig.S6B). Volcano plots further highlighted significant proteins with the largest $\log(\text{LFQ})$ difference (red and blue) for different pairwise comparisons, including ‘Dex-Spi vs EtOH’ (Fig. 7B), ‘Dex vs EtOH’ and ‘Spi vs EtOH’ (Supplementary Fig. S8A,C). Overrepresentation analyses of the Dex-Spi-regulated proteins identified that several hallmarks of metabolism, including oxidative phosphorylation and fatty acid metabolism, were significantly upregulated, while the hallmarks for cholesterol homeostasis, G2M checkpoint and E2F targets were significantly downregulated (Fig. 7C). Focusing on the individual hallmarks (Fig. 7D–G, Supplementary Fig.

S8E–H) demonstrated that only proteins regulated by Dex-Spi, and not by Dex or Spi, were significantly enriched for oxidative phosphorylation and fatty acid oxidation (Fig. 7D, E). Cholesterol homeostasis was inhibited by the Dex-Spi regulated proteins (Fig. 7F). In contrast, all treatments (Dex-Spi, Dex and Spi) gave rise to a significant enrichment of the G2M checkpoint and E2F targets, but it was Dex alone that inhibited these hallmarks the most (Fig. 7G, Supplementary Fig. 7E). In addition, the myc V2 hallmark was only significantly enriched upon Spi treatment in the proteomics analyses (Fig.S8G–H), while this enrichment was significant for all treatments in the RNA-sequencing analysis (Fig. 6H, I), which may be due to a difference in treatment time (6 h vs 24 h) in these experiments. Nonetheless, the master regulator c-myc was differentially regulated at the protein level (Fig. 6B).

Finally, we examined whether the expression levels of Dex-Spi-regulated proteins could predict survival in the CoMMpass cohort. The genes corresponding to the proteins that were uniquely up- or downregulated by Dex-Spi (upset plots, Supplementary Fig. 8E–F) were used as input as only transcriptomics data are available for the CoMMpass cohort. We found that patients having a low expression of the proteins uniquely downregulated by Dex-Spi had a better PFS and OS than patients having a high expression of these targets (Fig. 7H, Supplementary Fig.S9A). In contrast, high expression levels of proteins that were uniquely upregulated by Dex-Spi identified patients with worse PFS and OS (Fig. 7I, Supplementary Fig.S9B).

Summarized, on a mechanistic level, we additionally concluded that the Dex-Spi combination treatment deregulates several metabolic pathways.

Discussion

In this study, we have identified a novel, functionally relevant nuclear receptor crosstalk mechanism between GR and MR in myeloma cells (summarized in Fig. 7J). We have shown that although MR levels were decreased upon Dex treatment over time in a GR-dependent manner (A; Fig. 7J), endogenous GR strongly interacts with MR in a Dex-inducible manner at early stages (B; Fig. 7J). We further found that Spi clearly diminished Dex-induced GR–MR heterodimerization and completely abolished Dex-induced MR–MR homodimerization (B, Fig. 7J). Dex-Spi combination treatment also gave rise to a differential transcriptomic and proteomic signature (C; Fig. 7J) that can help explain the enhanced Dex-induced myeloma cell killing in combination with Spi (D; Fig. 7J). These four main findings will be discussed in further detail below.

We found that Dex downregulates MR levels likely by a superposition of different mechanisms. In earlier work,

GCs were reported to reduce the stability of pro-inflammatory mediators, such as $\text{TNF}\alpha$, by upregulating mediators of mRNA decay [54]. A similar mechanism decreased the *NR3C2* mRNA stability in renal epithelial cells subjected to hypertonic conditions [55], and recently several *NR3C2*-targeting miRNA's were identified in this context [56]. In myeloma cells, Dex did not further reduce the MR mRNA stability following ActD treatment (Fig. 1I). Pharmacological inhibition of transcription and translation rather supported that the Dex-induced decline of MR mRNA and protein depended, at least partially, on both mechanisms. Noteworthy, Dex treatment also induced a second MR band, approximately 10 kDa upwards, hinting at various post-translational modifications. Although an aldosterone-induced upward shift of MR of even 30 kDa was reported before, this was linked to increased phosphorylation on several serine residues with subsequent MR polyubiquitination and proteasomal degradation [57]. In the MM cell context, however, Dex did not decrease MR protein levels via proteasomal or lysosomal degradation (Supplementary Fig. S2B–E). Although GR was clearly required for the Dex-induced MR downregulation (Fig. 1B, F, G), an additional regulatory mechanism whereby GCs may directly bind to and affect MR, as in MM1.R cells that lack GR (Supplementary Fig. S2A), cannot be excluded.

We discovered that endogenous GR and MR may form heterodimers or are at least part of the same protein complex in myeloma cells. GR–MR heterodimerization and the formation of higher-order oligomers were reported before in different cell types [21, 24–26], although mostly using overexpressed receptors. Nonetheless, Number and Brightness studies, recently applied to GR–MR by the Alvarez de la Rosa team, offer the advantage of studying the receptors in real time in living cells [25]. Compared to typical nuclear receptor heterodimers (e.g. RXR and PPAR), atypical heterodimers such as GR–MR could be less prominent and transient, but that does not exclude a potentially strong functional effect [13]. GR and MR co-immunoprecipitated already in basal conditions (Fig. 5D, F), a finding that was reported before in untreated keratinocytes in which GR and MR were overexpressed [22]. GR–MR interaction was further supported by Dex via two orthogonal assay systems (Fig. 5B–G). Noteworthy is that Spi alone showed GR–MR interaction in the co-IP assays, albeit to a lower extent than Dex alone, while not at all in the NanoBiT assays (Fig. 5B versus 5D–G). This discrepancy may be due to the difference in assay conditions, as NanoBiT relies on overexpression of GR and MR and works in HEK293T kidney cells, while the co-IPs were performed in an endogenous context in myeloma cells where the levels of GR outweigh those of MR, as also shown in primary myeloma cells (Fig. 4N). An additional technology at the endogenous level, such as a proximity ligation assay (PLA) in myeloma cells, could

shed further light on the effect of Spi alone in future studies. Spi, however, consistently reduced Dex-induced GR–MR heterodimerization (Fig. 5B–G) and completely abolished MR–MR dimerization (Fig. 5J, K). A limitation of our work is that we only used a saturating concentration of 1 μM Dex in the MR homodimerization assay, mainly because this Dex concentration corresponds to clinically used doses in myeloma. Together, these results support a hypothesis that altered receptor dimerization equilibria may mechanistically contribute to an altered transcriptome and proteome profile and ultimately to the enhanced cell killing induced by the Dex–Spi combination. Besides direct, also indirect crosstalk mechanisms can affect the therapy response, as shown for GR and AR in prostate cancer, where even diminished responsiveness to enzalutamide (anti-androgen) was observed [14, 58]. Although the GR–MR crosstalk in MM1.S and OPM-2 cells may entail a direct physical interaction (Fig. 5B–E, H, I), further studies are necessary to discriminate between tethering-based interactions or cooperative DNA binding modes [24, 26] in the context of myeloma.

Transcriptome analysis has shown that Dex–Spi halted markers of transcription elongation. We found decreased Pol 2 Ser2 phosphorylation in MM1.S cells (Fig. 6B), which agrees with earlier work resolving tethering-based GR repression mechanisms in an inflammatory setting. There, Dex-activated GR hampered Pol 2 Ser2 phosphorylation at several NF- κB -regulated promoters [46]. In OPM-2 cells, increased expression of the transcriptional repressor HEXIM1 appeared more decisive for a Dex–Spi-induced block in transcription elongation (Fig. 6B). The latter findings agree with a study where HEXIM1 sequestered positive transcription elongation factor b (P-TEFb) to inhibit transcription elongation of tumorigenic genes [47]. In line, Rogatsky and colleagues demonstrated that GR can even inhibit recruitment of the P-TEFb complex that is normally responsible for Pol 2 Ser2 phosphorylation [59]. Altogether, Dex–Spi consistently triggers several (consecutive) steps to inhibit transcription in GC-sensitive MM cells, regardless of cell-line specific regulations of the underlying markers.

Furthermore, our results strongly suggest that c-myc and many of its target genes (Figs. 5H, I, 6B) may be responsible for the enhanced myeloma cell killing induced by Dex–Spi. The fact that GCs decrease c-myc levels is well documented in the literature [48, 60] and results in cell cycle arrest at the G1 phase in leukemia cells [60]; even Spi alone was linked to decreased c-myc activity before [61]. In myeloma, reports show that c-myc protein was overexpressed in 40% of patients at diagnosis, which correlated with shorter OS [45]. Moreover, in 2022, the team of Rosen showed that inhibiting SUMOylation in myeloma cells resulted in decreased c-myc protein stability, which in turn decreased the levels of several miRNAs involved in either GR downregulation or GC resistance [62]. Using survival analyses on the CoMMpass patient

cohort (Fig. 6J, K), we further found that patients have a lower risk of progression when displaying low levels of the unique Dex-Spi-downregulated genes, which may altogether be predictive of the clinical relevance of a combination treatment. In addition, patients having high MR expression levels at diagnosis showed superior OS, while GR expression levels were not predictive for survival (Fig. 4O, P). For GR, this contrasts a previous study, where high expression levels at diagnosis were found predictive for OS [63]. One reason for this difference may be that Rosen and colleagues stratified patients in two subgroups, based on whether they underwent stem cell transplantation or not, and another reason may be that at that time only version IA13 of the database was available (with 650 patients vs. IA14 with 750 patients).

Our study of the proteome additionally revealed that metabolic hallmarks such as oxidative phosphorylation and fatty acid metabolism were upregulated, while the hallmark cholesterol homeostasis was downregulated most by the Dex-Spi combination treatment (Fig. 7D-F). Reports in several lymphoid malignant cell types have associated enhanced metabolism, i.e. increased glycolysis, oxidative phosphorylation, cholesterol biosynthesis and fatty acid oxidation, with decreased GC responsiveness or even GC resistance [64–66]. In ALL cells, GCs inhibited glycolysis, which was not sufficient to trigger cell death but did induce a metabolic shift to mitochondrial oxidative phosphorylation to obtain survival energy [67]. In line with this, combining GCs with the oxidative phosphorylation inhibitor oligomycin sensitized GC-resistant ALL cells to cell killing [65]. This team also found synergistic cell killing in GC-resistant ALL cell lines when GCs were combined with an inhibitor of cholesterol metabolism (simvastatin) [65]. In CLL cells, GCs reduce metabolic activity among others by downregulating pyruvate kinase M2 and decreasing levels of pyruvate. Concomitantly however, this elevated the dependency of the CLL cells on fatty acid oxidation because GCs also upregulated PPAR α and PDK4 expression [66]. Based on these studies, increased oxidative phosphorylation and fatty acid metabolism may be rather an unwanted feature of the Dex-Spi combination treatment in a context of prolonged treatment, although this requires further investigation. Within this context, our survival analysis (Fig. 7I) supports that high expression of proteins that were uniquely upregulated by Dex-Spi was indeed associated with worse PFS. In contrast, the marked inhibition of cholesterol homeostasis observed solely with Dex-Spi treatment may rather be a contributing mechanism that can drive and explain the enhanced myeloma cell killing. Nonetheless, the connection between GCs and potential shifts in metabolism in myeloma cells, especially in the context of prolonged treatment, is rather understudied, which opens opportunities for follow-up research.

Concerning markers mimicking GC-related side effects, we have shown that REDD1 (*DDIT4*), an instigator of

myeloma cell growth and survival [50], is decreased by Dex-Spi combination compared to Dex in MM1.S and OPM-2 (Fig. 6D). Because GC-mediated increases in REDD1 levels were also shown to contribute to muscle atrophy [68], this suggests that Dex-Spi may perhaps improve GC-induced muscle atrophy. Whether those and other metabolic side effects could also be improved at the organism level remains to be investigated in follow-up studies.

We discovered that Spi enhances Dex-induced cell killing of myeloma cells, i.e., in GC-sensitive MM1.S and OPM-2 cells as well as in patient cells of several newly diagnosed patients and a smoldering MM patient (Figs. 2, 3A, 4A, B, K). Our findings agree with a study in which a GC-treated pre-B lymphoma cell line stably overexpressing the N-terminal domain (NTD) of MR resulted in blocked apoptosis [28]. In our case, Spi addition partially suppressed Dex-induced GR–MR heterodimer formation and abolished Dex-induced MR–MR homodimerization, which may form a molecular basis to support differential gene and protein expression profiles with enhanced anti-myeloma outcomes compared to Dex. Noteworthy, Spi is a potent FDA-approved MR antagonist, however, less selective because it causes anti-androgenic (via AR) and progestogenic (via progesterone receptor, PR) side effects as well as hyperkalemia [17]. A limitation of our study is that we did not include a more selective MR antagonist, such as Eplerenone, mainly because this compound has a 40-fold lower affinity for MR than Spi [17]. In follow-up work, the non-steroidal, potent and selective MR antagonist finerenone can be considered [69] to examine whether improved selectivity also gives rise to enhanced Dex-induced myeloma cell killing. Spi did at least not require GR for its action, because GR-negative MM1.R cells underwent ~30% cell killing upon Spi treatment (Fig. 3D). In these GC-resistant, MR-positive MM1.R cells, the myeloma cell killing effect of Spi was also substantially larger than in U-266 cells (Fig. 3C, D), which express low levels of MR, suggesting that Spi acts at least in part in an MR-dependent way. Nonetheless, reports show that Spi by itself can suppress pro-inflammatory cytokines and induce apoptosis in blood mononuclear cells by reducing NF- κ B and c-myc activities [61]. Spi was also found to inhibit nucleotide excision repair which resulted in increased sensitivity of (primary) myeloma cells to alkylating agents such as melphalan [70]. A final limitation of our study is that we cannot exclude that MR-independent actions are partially underlying the Spi-induced myeloma cell killing. Therefore, follow-up work should include more selective MR antagonists and examine whether MR agonists protect against Dex-mediated myeloma cell killing. Our study nonetheless supports a marked reduction in cell viability observed upon 10^{-5} M Spi monotherapy across all (patient-derived) MM cells (Figs. 2, 3, 4).

In conclusion, our results support the high potential of MR as an additional therapeutic target in myeloma, of which antagonists may be repurposed for myeloma treatment in combination with GCs as add-on to the myeloma standard of care treatment. We showed that a functional crosstalk between GR and MR exists in myeloma and that a targeting hereof with ligands warrants further investigation of its potential therapeutic benefit in terms of efficacy, safety and the possibility to reduce the GC-dose.

Supplementary Information The online version contains supplementary material available at <https://doi.org/10.1007/s00018-023-04900-x>.

Author contributions DC performed conceptualization, investigation, data curation, formal analysis, validation, visualization, methodology, writing—original draft, and writing—review and editing. SP contributed to investigation, data curation, formal analysis, visualization, writing—review and editing. PV was involved in data curation, writing—review and editing. ES contributed to investigation and writing—review and editing. KVV was involved in investigation. JT performed investigation and formal analysis. DF contributed to data curation, formal analysis, and writing—review and editing. GA performed data curation, formal analysis, visualization, and writing—review and editing. WZ contributed to writing—review and editing. IMB was involved in conceptualization, writing—review and editing, and supervision. FO contributed to writing—review and editing and supervision. KDB was involved in conceptualization, writing—review and editing, and supervision.

Funding DC was funded by a predoctoral fellowship from Flanders Innovation and Entrepreneurship (VLAIO), grant number 131374 (www.vlaio.be) until December 2017. Research project funded by Kom op tegen Kanker (Stand up to Cancer), the Flemish cancer society (grant numbers KDB 2012-VLK-GC-MM and STI.VLK.2018.0019.01). This work was further supported through VIB and Ghent University institutional funding to KDB.

Data availability The datasets used in this study are available in the following databases: RNA-seq data in the Gene Expression Omnibus (GEO) database with accession number GSE200313; the mass spectrometry proteomics data have been deposited to the ProteomeXchange Consortium via the Proteomics Identification (PRIDE) partner repository with the dataset identifier PXD043635.

Declarations

Conflict of interest The authors have no relevant financial or non-financial interests to disclose.

Consent to participate Informed consent was obtained from all patients included in the study.

Open Access This article is licensed under a Creative Commons Attribution 4.0 International License, which permits use, sharing, adaptation, distribution and reproduction in any medium or format, as long as you give appropriate credit to the original author(s) and the source, provide a link to the Creative Commons licence, and indicate if changes were made. The images or other third party material in this article are included in the article's Creative Commons licence, unless indicated otherwise in a credit line to the material. If material is not included in the article's Creative Commons licence and your intended use is not permitted by statutory regulation or exceeds the permitted use, you will

need to obtain permission directly from the copyright holder. To view a copy of this licence, visit <http://creativecommons.org/licenses/by/4.0/>.

References

- Rajkumar SV (2022) Multiple myeloma: 2022 update on diagnosis, risk stratification, and management. *Am J Hematol* 97:1086–1107. <https://doi.org/10.1002/ajh.26590>
- Burwick N, Sharma S (2019) Glucocorticoids in multiple myeloma: past, present, and future. *Ann Hematol* 98:19–28. <https://doi.org/10.1007/s00277-018-3465-8>
- Clarisse D, Offner F, De Bosscher K (2020) Latest perspectives on glucocorticoid-induced apoptosis and resistance in lymphoid malignancies. *Biochim Biophys Acta Rev Cancer* 1874:188430. <https://doi.org/10.1016/j.bbcan.2020.188430>
- Weikum ER, Liu X, Ortlund EA (2018) The nuclear receptor superfamily: a structural perspective. *Protein Sci* 27:1876–1892. <https://doi.org/10.1002/pro.3496>
- Moessmer P, Suren T, Majdic U et al (2022) Active unfolding of the glucocorticoid receptor by the Hsp70/Hsp40 chaperone system in single-molecule mechanical experiments. *Proc Natl Acad Sci USA* 119:e2119076119. <https://doi.org/10.1073/pnas.2119076119>
- Vandewalle J, Luypaert A, De Bosscher K, Libert C (2018) Therapeutic mechanisms of glucocorticoids. *Trends Endocrinol Metab* 29:42–54. <https://doi.org/10.1016/j.tem.2017.10.010>
- John S, Sabo PJ, Thurman RE et al (2011) Chromatin accessibility pre-determines glucocorticoid receptor binding patterns. *Nat Genet* 43:264–268. <https://doi.org/10.1038/ng.759>
- Timmermans S, Souffriau J, Libert C (2019) A general introduction to glucocorticoid biology. *Front Immunol* 10:1545. <https://doi.org/10.3389/fimmu.2019.01545>
- Love MI, Huska MR, Jurk M et al (2017) Role of the chromatin landscape and sequence in determining cell type-specific genomic glucocorticoid receptor binding and gene regulation. *Nucleic Acids Res* 45:1805–1819. <https://doi.org/10.1093/nar/gkw1163>
- Sacta MA, Tharmalingam B, Coppo M et al (2018) Gene-specific mechanisms direct glucocorticoid-receptor-driven repression of inflammatory response genes in macrophages. *Elife* 7:1–25. <https://doi.org/10.7554/eLife.34864>
- Paakinaho V, Johnson TA, Presman DM, Hager GL (2019) Glucocorticoid receptor quaternary structure drives chromatin occupancy and transcriptional outcome. *Genome Res* 29:1223–1234. <https://doi.org/10.1101/gr.244814.118>
- Johnson TA, Paakinaho V, Kim S et al (2021) Genome-wide binding potential and regulatory activity of the glucocorticoid receptor's monomeric and dimeric forms. *Nat Commun* 12:1987. <https://doi.org/10.1038/s41467-021-22234-9>
- De Bosscher K, Desmet SJ, Clarisse D et al (2020) Nuclear receptor crosstalk—defining the mechanisms for therapeutic innovation. *Nat Rev Endocrinol* 16:363–377. <https://doi.org/10.1038/s41574-020-0349-5>
- Paakinaho V, Palvimo JJ (2021) Genome-wide crosstalk between steroid receptors in breast and prostate cancers. *Endocr Relat Cancer* 28:R231–R250. <https://doi.org/10.1530/ERC-21-0038>
- Devlies W, Handle F, Devos G et al (2021) Preclinical models in prostate cancer: resistance to AR targeting therapies in prostate cancer. *Cancers* 13:915. <https://doi.org/10.3390/cancers13040915>
- Gomez-Sanchez E, Gomez-Sanchez CE (2014) The multifaceted mineralocorticoid receptor. *Compr Physiol* 4:965–994. <https://doi.org/10.1002/cphy.c130044>
- Clarisse D, Deng L, Bosscher K, Lothar A (2021) Approaches towards tissue-selective pharmacology of the mineralocorticoid receptor. *Br J Pharmacol*. <https://doi.org/10.1111/bph.15719>

18. Agarwal R, Kolkhof P, Bakris G et al (2021) Steroidal and non-steroidal mineralocorticoid receptor antagonists in cardiorenal medicine. *Eur Heart J* 42:152–161. <https://doi.org/10.1093/eurheartj/ehaa736>
19. Pearce D, Yamamoto KR (1993) Mineralocorticoid and glucocorticoid receptor activities distinguished by nonreceptor factors at a composite response element. *Science* 259:1161–1165. <https://doi.org/10.1126/science.8382376>
20. Le Billan F, Amazit L, Bleakley K et al (2018) Corticosteroid receptors adopt distinct cyclical transcriptional signatures. *FASEB J* 32:5626–5639. <https://doi.org/10.1096/fj.201800391RR>
21. Mifsud KR, Reul JM (2016) Acute stress enhances heterodimerization and binding of corticosteroid receptors at glucocorticoid target genes in the hippocampus. *Proc Natl Acad Sci* 113:11336–11341. <https://doi.org/10.1073/pnas.1605246113>
22. Bigas J, Sevilla LM, Carceller E et al (2018) Epidermal glucocorticoid and mineralocorticoid receptors act cooperatively to regulate epidermal development and counteract skin inflammation. *Cell Death Dis* 9:1–14. <https://doi.org/10.1038/s41419-018-0673-z>
23. Carceller-Zazo E, Sevilla LM, Pons-Alonso O et al (2023) The mineralocorticoid receptor modulates timing and location of genomic binding by glucocorticoid receptor in response to synthetic glucocorticoids in keratinocytes. *FASEB J* 37:e22709. <https://doi.org/10.1096/fj.202201199RR>
24. Pooley JR, Rivers CA, Kilcooley MT et al (2020) Beyond the heterodimer model for mineralocorticoid and glucocorticoid receptor interactions in nuclei and at DNA. *PLoS ONE* 15:e0227520. <https://doi.org/10.1371/journal.pone.0227520>
25. Fettweis G, Johnson TA, Almeida-Prieto B, et al (2023) The mineralocorticoid receptor forms higher order oligomers upon DNA binding. 2023.01.26.525752
26. Rivers CA, Rogers MF, Stubbs FE et al (2019) Glucocorticoid receptor tethered mineralocorticoid receptors increase glucocorticoid-induced transcriptional responses. *Endocrinology* 160:1044–1056. <https://doi.org/10.1210/en.2018-00819>
27. Derfoul A, Robertson NM, Hall DJ, Litwack G (2000) The N-terminal domain of the mineralocorticoid receptor modulates both mineralocorticoid receptor- and glucocorticoid receptor-mediated transactivation from Na/K ATPase beta1 target gene promoter. *Endocrine* 13:287–295. <https://doi.org/10.1385/ENDO:13:3:287>
28. Planey SL, Derfoul A, Steplewski A et al (2002) Inhibition of glucocorticoid-induced apoptosis in 697 pre-B lymphocytes by the mineralocorticoid receptor N-terminal domain. *J Biol Chem* 277:42188–42196. <https://doi.org/10.1074/jbc.M205085200>
29. Küllerich P, Triqueneaux G, Christensen NM et al (2015) Interaction between the trout mineralocorticoid and glucocorticoid receptors in vitro. *J Mol Endocrinol* 55:55–68. <https://doi.org/10.1530/jme-15-0002>
30. Subramanian A, Tamayo P, Mootha VK et al (2005) Gene set enrichment analysis: a knowledge-based approach for interpreting genome-wide expression profiles. *Proc Natl Acad Sci* 102:15545–15550. <https://doi.org/10.1073/pnas.0506580102>
31. Clarisse D, Van Wesemael K, Tavernier J et al (2018) Effect of combining glucocorticoids with compound a on glucocorticoid receptor responsiveness in lymphoid malignancies. *PLoS ONE* 13:1–17. <https://doi.org/10.1371/journal.pone.0197000>
32. Prekovic S, Schuurman K, Mayayo-Peralta I et al (2021) Glucocorticoid receptor triggers a reversible drug-tolerant dormancy state with acquired therapeutic vulnerabilities in lung cancer. *Nat Commun* 12:4360. <https://doi.org/10.1038/s41467-021-24537-3>
33. Clarisse D, Thommis J, Van Wesemael K et al (2017) Coregulator profiling of the glucocorticoid receptor in lymphoid malignancies. *Oncotarget* 8:109675–109691. <https://doi.org/10.18632/oncotarget.22764>
34. Greenstein S, Krett NL, Kurosawa Y et al (2003) Characterization of the MM.1 human multiple myeloma (MM) cell lines: a model system to elucidate the characteristics, behavior, and signaling of steroid-sensitive and -resistant MM cells. *Exp Hematol* 31:271–282. [https://doi.org/10.1016/S0301-472X\(03\)00023-7](https://doi.org/10.1016/S0301-472X(03)00023-7)
35. Kervoëlen C, Ménoret E, Gomez-Bougie P et al (2015) Dexamethasone-induced cell death is restricted to specific molecular subgroups of multiple myeloma. *Oncotarget* 6:26922–26934. <https://doi.org/10.18632/oncotarget.4616>
36. Bachmann PS, Gorman R, Papa RA et al (2007) Divergent mechanisms of glucocorticoid resistance in experimental models of pediatric acute lymphoblastic leukemia. *Can Res* 67:4482–4490. <https://doi.org/10.1158/0008-5472.CAN-06-4244>
37. Sanchez-Vega B, Gandhi V (2009) Glucocorticoid resistance in a multiple myeloma cell line is regulated by a transcription elongation block in the glucocorticoid receptor gene (NR3C1). *Br J Haematol* 144:856–864. <https://doi.org/10.1111/j.1365-2141.2008.07549.x>
38. Ramamoorthy S, Cidlowski JA (2013) Ligand-induced repression of the glucocorticoid receptor gene is mediated by an NCoR1 repression complex formed by long-range chromatin interactions with intragenic glucocorticoid response elements. *Mol Cell Biol* 33:1711–1722. <https://doi.org/10.1128/MCB.01151-12>
39. Ayroldi E, Riccardi C (2009) Glucocorticoid-induced leucine zipper (GILZ): a new important mediator of glucocorticoid action. *FASEB J* 23:3649–3658. <https://doi.org/10.1096/fj.09-134684>
40. Gadasheva Y, Nolze A, Grossmann C (2021) Posttranslational modifications of the mineralocorticoid receptor and cardiovascular aging. *Front Mol Biosci*. <https://doi.org/10.3389/fmolb.2021.667990>
41. Fagerli U-M, Ullrich K, Stühmer T et al (2011) Serum/glucocorticoid-regulated kinase 1 (SGK1) is a prominent target gene of the transcriptional response to cytokines in multiple myeloma and supports the growth of myeloma cells. *Oncogene* 30:3198–3206. <https://doi.org/10.1038/ncr.2011.79>
42. Fries GR, Gassen NC, Rein T (2017) The FKBP51 glucocorticoid receptor co-chaperone: regulation, function, and implications in health and disease. *Int J Mol Sci* 18:1–31. <https://doi.org/10.3390/ijms18122614>
43. Mizuhashi K, Kanamoto T, Ito M et al (2012) OBIF, an osteoblast induction factor, plays an essential role in bone formation in association with osteoblastogenesis. *Dev Growth Differ* 54:474–480. <https://doi.org/10.1111/j.1440-169X.2012.01333.x>
44. Huntley R, Jensen E, Gopalakrishnan R, Mansky KC (2019) Bone morphogenetic proteins: their role in regulating osteoclast differentiation. *Bone Rep* 10:100207. <https://doi.org/10.1016/j.bonr.2019.100207>
45. Szabo AG, Gang AO, Pedersen MØ et al (2016) Overexpression of c-myc is associated with adverse clinical features and worse overall survival in multiple myeloma. *Leuk Lymphoma* 57:2526–2534. <https://doi.org/10.1080/10428194.2016.1187275>
46. Nissen RM, Yamamoto KR (2000) The glucocorticoid receptor inhibits NFκB by interfering with serine-2 phosphorylation of the RNA polymerase II carboxy-terminal domain. *Genes Dev* 14:2314–2329. <https://doi.org/10.1101/gad.827900>
47. Tan JL, Fogley RD, Flynn RA et al (2016) Stress from nucleotide depletion activates the transcriptional regulator HEXIM1 to suppress melanoma. *Mol Cell* 62:34–46. <https://doi.org/10.1016/j.molcel.2016.03.013>
48. Rogatsky I, Trowbridge JM, Garabedian MJ (1997) Glucocorticoid receptor-mediated cell cycle arrest is achieved through distinct cell-specific transcriptional regulatory mechanisms. *Mol Cell Biol* 17:3181–3193. <https://doi.org/10.1128/MCB.17.6.3181>
49. Vallet S, Pozzi S, Patel K et al (2011) A novel role for CCL3 (MIP-1α) in myeloma-induced bone disease via osteocalcin downregulation and inhibition of osteoblast function. *Leukemia* 25:1174–1181. <https://doi.org/10.1038/leu.2011.43>

50. Decaux O, Clément M, Magrangeas F et al (2010) Inhibition of mTORC1 activity by REDD1 induction in myeloma cells resistant to bortezomib cytotoxicity. *Cancer Sci* 101:889–897. <https://doi.org/10.1111/j.1349-7006.2009.01467.x>
51. Britto FA, Begue G, Rossano B et al (2014) REDD1 deletion prevents dexamethasone-induced skeletal muscle atrophy. *Am J Physiol Endocrinol Metab* 307:E983–E993. <https://doi.org/10.1152/ajpendo.00234.2014>
52. Harnoss JM, Thomas AL, Shemorry A et al (2019) Disruption of IRE1 α through its kinase domain attenuates multiple myeloma. *PNAS* 116:16420–16429. <https://doi.org/10.1073/pnas.1906999116>
53. De Matos SR, Shirasaki R, Tang H et al (2020) POU2AF1 as a master regulator of oncogenic transcription factor networks in myeloma. *Blood* 136:18–19. <https://doi.org/10.1182/blood-2020-142580>
54. Smoak K, Cidlowski JA (2006) Glucocorticoids regulate tristetraprolin synthesis and posttranscriptionally regulate tumor necrosis factor alpha inflammatory signaling. *Mol Cell Biol* 26:9126–9135. <https://doi.org/10.1128/MCB.00679-06>
55. Viengchareun S, Lema I, Lamribet K et al (2014) Hypertonicity compromises renal mineralocorticoid receptor signaling through Tis11b-mediated post-transcriptional control. *J Am Soc Nephrol* 25:2213–2221. <https://doi.org/10.1681/ASN.2013091023>
56. Vu TA, Lema I, Hani I et al (2022) miR-324-5p and miR-30c-2-3p alter renal mineralocorticoid receptor signaling under hypertonicity. *Cells* 11:1377. <https://doi.org/10.3390/cells11091377>
57. Faresse N, Vitagliano J-J, Staub O (2012) Differential ubiquitylation of the mineralocorticoid receptor is regulated by phosphorylation. *FASEB J* 26:4373–4382. <https://doi.org/10.1096/fj.12-209924>
58. Isikbay M, Otto K, Kregel S et al (2014) Glucocorticoid receptor activity contributes to resistance to androgen-targeted therapy in prostate cancer. *Hormones and Cancer* 5:72–89. <https://doi.org/10.1007/s12672-014-0173-2>
59. Gupte R, Muse GW, Chinenov Y et al (2013) Glucocorticoid receptor represses proinflammatory genes at distinct steps of the transcription cycle. *PNAS* 110:14616–14621. <https://doi.org/10.1073/pnas.1309898110>
60. Ausserlechner M, Obexer P, Böck G et al (2004) Cyclin D3 and c-MYC control glucocorticoid-induced cell cycle arrest but not apoptosis in lymphoblastic leukemia cells. *Cell Death Differ* 11:165–174. <https://doi.org/10.1038/sj.cdd.4401328>
61. Sønnder S, Mikkelsen M, Rieneck K et al (2006) Effects of spironolactone on human blood mononuclear cells: mineralocorticoid receptor independent effects on gene expression and late apoptosis induction. *Br J Pharmacol* 148:46–53. <https://doi.org/10.1038/sj.bjp.0706700>
62. Du L, Liu W, Aldana-Masangkay G et al (2022) SUMOylation inhibition enhances dexamethasone sensitivity in multiple myeloma. *J Exp Clin Cancer Res* 41:8. <https://doi.org/10.1186/s13046-021-02226-9>
63. Pozhitkov A, Rosenzweig M, Pichiorri F et al (2020) Glucocorticoid receptor expression in multiple myeloma patients is a predictor of survival. *Leukem Lymphoma*. <https://doi.org/10.1080/10428194.2020.1811860>
64. Beesley A, Firth M, Ford J et al (2009) Glucocorticoid resistance in T-lineage acute lymphoblastic leukaemia is associated with a proliferative metabolism. *Br J Cancer* 100:1926–1936. <https://doi.org/10.1038/sj.bjc.6605072>
65. Samuels AL, Heng JY, Beesley AH, Kees UR (2014) Bioenergetic modulation overcomes glucocorticoid resistance in T-lineage acute lymphoblastic leukaemia. *Br J Haematol* 165:57–66. <https://doi.org/10.1111/bjh.12727>
66. Tung S, Shi Y, Wong K et al (2013) PPAR α and fatty acid oxidation mediate glucocorticoid resistance in chronic lymphocytic leukemia. *Blood* 122:969–980. <https://doi.org/10.1182/blood-2013-03-489468>
67. Aoki S, Morita M, Hirao T, Yamaguchi M (2017) Shift in energy metabolism caused by glucocorticoids enhances the effect of cytotoxic anti-cancer drugs against acute lymphoblastic leukemia cells. *Oncotarget* 8:94271–94285. <https://doi.org/10.18632/oncotarget.21689>
68. Sandri M, Sandri C, Gilbert A et al (2004) Foxo transcription factors induce the atrophy-related ubiquitin ligase atrogin-1 and cause skeletal muscle atrophy. *Cell* 117:1–2. [https://doi.org/10.1016/S0092-8674\(04\)00400-3](https://doi.org/10.1016/S0092-8674(04)00400-3)
69. Bärfacker L, Kuhl A, Hillisch A et al (2012) Discovery of BAY 94–8862: a nonsteroidal antagonist of the mineralocorticoid receptor for the treatment of cardiorenal diseases. *ChemMedChem* 7:1385–1403. <https://doi.org/10.1002/cmdc.201200081>
70. Szalat R, Samur MK, Fulciniti M et al (2018) Nucleotide excision repair is a potential therapeutic target in multiple myeloma. *Leukemia* 32:111–119. <https://doi.org/10.1038/leu.2017.182>

Publisher's Note Springer Nature remains neutral with regard to jurisdictional claims in published maps and institutional affiliations.